

Testing the isomorph invariance of the bridge functions of Yukawa one-component plasmas

Cite as: J. Chem. Phys. 154, 034501 (2021); doi: 10.1063/5.0036226

Submitted: 3 November 2020 • Accepted: 29 December 2020 •

Published Online: 19 January 2021



View Online



Export Citation



CrossMark

F. Lucco Castello,^{1,a)} P. Tolias,¹ and J. C. Dyre²

AFFILIATIONS

¹Space and Plasma Physics, Royal Institute of Technology, Stockholm SE-100 44, Sweden

²Glass and Time, IMFUFA, Roskilde University, Roskilde DK-4000, Denmark

^{a)}Author to whom correspondence should be addressed: flc@kth.se

ABSTRACT

It has been recently conjectured that bridge functions remain nearly invariant along phase diagram lines of constant excess entropy for the broad class of R-simple liquids. To test this hypothesis, the bridge functions of Yukawa systems are computed outside the correlation void with the Ornstein–Zernike inversion method employing structural input from ultra-accurate molecular dynamics simulations and inside the correlation void with the cavity distribution method employing structural input from ultra-long specially designed molecular dynamics simulations featuring a tagged particle pair. Yukawa bridge functions are revealed to be isomorph invariant to a very high degree. The observed invariance is not exact, however, since isomorph deviations exceed the overall uncertainties.

© 2021 Author(s). All article content, except where otherwise noted, is licensed under a Creative Commons Attribution (CC BY) license (<http://creativecommons.org/licenses/by/4.0/>). <https://doi.org/10.1063/5.0036226>

I. INTRODUCTION

One of the fundamental problems in the statistical mechanics of liquids concerns the accurate computation of static pair correlations with the knowledge of the pair interaction potential alone and without resorting to computer simulations. The integral equation theory of liquids features two formally exact equations for this problem that contain three unknown functions; an additional equation for the so-called bridge function is missing.^{1–4} The unknown bridge function incorporates all the elements that make a many body problem of infinite degrees of freedom unsolvable. Therefore, it is not surprising that its diagrammatic expansion is very slowly converging and its high-order terms quickly become overly complicated to calculate.⁵ As a consequence, numerous approximation schemes have been developed for the bridge function, whose effectiveness varies depending on the potential and can only be reliably evaluated *a posteriori* through a comparison with “exact” simulation results.^{1,6,7} It is fortuitous, though, that static correlations in liquids exhibit relatively weak dependence on the bridge function.¹

Contrary to the radial distribution function, the bridge function possesses neither a microscopic representation (in terms of

δ -functions and instantaneous particle positions) nor a conditional probability interpretation. Thus, the bridge function cannot be directly extracted from computer simulations. Nevertheless, it can be computed with input from computer simulations. In particular, the extraction of radial distribution functions leads to the closure of the system of integral equation theory and allows one to solve for the unknown bridge function. There are two caveats with such an indirect extraction method. First, the weak dependence of static correlations on the bridge function implies a strong sensitivity of the bridge function to the radial distribution function; in other words, what is an asset in the direct problem becomes an obstacle in the inverse problem, which necessitates long simulations with a large particle number. Second, irrespective of the achieved size of the statistical sample, the inversion method is doomed to fail at very short distances where the probability of encountering another particle is ultra-low (for finite thermodynamically stable potentials) or is even zero (for unbounded potentials). Cavity simulations featuring a special tagged particle pair and utilizing umbrella sampling techniques have been conceived for the computation of the bridge function at such distances.⁸

Despite the inherent numerical difficulties of the computational procedure, “exact” bridge functions have been computed with

structural input from Monte Carlo (MC) or molecular dynamics (MD) simulations for different established model potentials such as hard-sphere systems^{8–11} and their binary mixtures,^{9,11} Lennard-Jones systems,^{12–15} inverse power law (IPL) systems,^{16,17} and one-component plasma liquids.^{18–20} In addition, “exact” bridge functions have been obtained for more realistic liquids including isotropic hard spheroid fluids,²¹ liquid metal model inter-ionic potentials,²² model 2–2 electrolytes,²³ molten salts,²⁴ Lennard-Jones dipolar fluids,²⁵ and even the extended simple point charge (SPC/E) site–site model of water.²⁶

Despite the undeniable progress during half a century of investigations, few exact or approximate properties of bridge functions have so far been discovered. Recently, a novel integral equation theory approach has been formulated that is based on the conjecture that bridge functions remain invariant along phase diagram lines of constant excess entropy for a broad class of liquids known as R-simple.²⁷ It has been coined as isomorph-based empirically modified hypernetted-chain (IEMHNC) and has been applied to Yukawa and bi-Yukawa liquids resulting in a remarkable agreement with simulations.^{27–29}

The primary objective of the present investigation is to test the validity of the underlying ansatz of bridge function invariance for Yukawa one-component plasmas (YOCPs).³⁰ The intermediate and long range Yukawa bridge functions will be computed along different isentropic lines with input from ultra-accurate standard MD simulations, and the short range Yukawa bridge functions will be computed with input from ultra-long specially designed MD simulations featuring a tagged particle pair. It should be emphasized that Yukawa systems have been selected as a representative system, but the conclusions of this case study are anticipated to be valid for all R-simple liquids. In the same spirit, the guidelines proposed for the optimal design of the simulations, the algorithmic procedure developed for the design of the tagged particle interaction potential, and the methodological approach suggested for the quantification of bridge function uncertainties are of generic nature and, thus, relevant to any dense liquid.

This paper is organized as follows. Section II features an introduction to Yukawa one-component plasmas, isomorph theory, and R-simple systems and discusses arguments in favor of the isomorph invariance of bridge functions. In Sec. III, 16 Yukawa state points are identified with isomorph tracing techniques and distributed among four isomorphs. In Sec. IV, the physics ideas behind indirect bridge function extraction techniques are discussed. In Sec. V, the Ornstein–Zernike (OZ) inversion method is presented, simulation parameters are specified, and bridge functions are computed outside the correlation void. In Sec. VI, the cavity distribution method is presented, simulation parameters are specified, and bridge functions are computed within the correlation void and extrapolated at the origin. In Sec. VII, the results are summarized.

II. BACKGROUND

For the present article to be self-contained, following a brief introduction to the standard nomenclature of the Yukawa one-component plasmas, a concise primer focusing on the isomorph theory of R-simple systems and the isomorph-based empirically

modified hypernetted-chain approach is given in the present section. The reader is addressed to the references cited below for further details.

A. Yukawa one-component plasmas

Yukawa one-component plasma (YOCP) systems are model systems whose constituents are charged point particles that are immersed in a neutralizing background and interact via the screened Coulomb (Yukawa) pair potential $u(r) = (Q^2/r) \exp(-r/\lambda)$, where Q is the particle charge and λ is the screening length determined by the polarizable background. It is convenient to specify the thermodynamic state points of the YOCP in terms of two independent dimensionless variables, the coupling parameter Γ and the screening parameter κ defined by^{32–35}

$$\Gamma = \beta \frac{Q^2}{d}, \quad \kappa = \frac{d}{\lambda}.$$

Here, $\beta = 1/(k_B T)$, with k_B being the Boltzmann constant and T being the temperature, and $d = (4\pi n/3)^{-1/3}$ stands for the Wigner–Seitz radius, with n being the particle (number) density.

In the limit of a rigid background $\lambda \rightarrow \infty$ or $\kappa \rightarrow 0$, the Yukawa potential collapses to the unscreened Coulomb potential and the resulting model system is then known as the one-component plasma (OCP). The YOCP enables the exploration of the full range of potential softness from the long range Coulomb interactions of the OCP for $\kappa = 0$ to ultra-short range hard-sphere interactions for $\kappa \rightarrow \infty$. Due to its variable softness and its relevance to strongly coupled laboratory systems such as complex plasmas and colloidal suspensions,^{36,37} the YOCP is still being actively investigated in statistical mechanics studies.

It is worth noting that the distances are typically normalized by the Wigner–Seitz radius $d = (4\pi n/3)^{-1/3}$ in the non-ideal plasma literature, while the distances are typically normalized by the mean-cubic inter-particle distance $\Delta = n^{-1/3}$ in the liquid state and isomorph theory literature. Both normalizations will be used in the present work, but mainly the plasma normalization to remain consistent with the screening parameter definition.

B. Isomorph theory and R-simple systems

Isomorphic lines or simply *isomorphs* are phase diagram curves of constant excess entropy, along which a large set of structural and dynamic properties are approximately invariant when expressed in properly reduced units.^{38–41} In case of Newtonian dynamics, the length is normalized to the mean-cubic inter-particle distance $\Delta = n^{-1/3}$, the energy is normalized to the thermal energy $k_B T$, and the time is normalized to the time required for a particle that is free streaming with its thermal velocity to traverse an inter-particle distance $\tau = n^{-1/3} \sqrt{m/(k_B T)}$.⁴¹ All systems have isentropic curves in their thermodynamic phase diagram, but these are termed isomorphs only for the so-called Roskilde-simple or R-simple systems.

R-simple systems are rigorously defined as many body systems that possess the property that the ordering of the total potential energies of two configurations consistent with the same density is maintained when these two configurations are uniformly scaled to

a different density.⁴² Mathematically, $U(\mathbf{R}_a) < U(\mathbf{R}_b) \Rightarrow U(\mu\mathbf{R}_a) < U(\mu\mathbf{R}_b)$ for positive μ , where $U(\mathbf{R})$ is the total potential energy, \mathbf{R} is the particle configuration that is given by the collective N -particle position vector $(\mathbf{r}_1, \dots, \mathbf{r}_N)$, and $\mathbf{R}_a, \mathbf{R}_b$ denote two equal density configurations.⁴² The hidden scale invariance property is exact only for systems that are characterized by Euler-homogeneous interactions (plus a constant), such as inverse power law (IPL) systems. For other R-simple systems, hidden scale invariance should be understood to be valid for most of the physically relevant configurations reflecting the approximate nature of isomorph theory.

R-simple systems are practically identified as systems possessing strong correlations between their virial (W) and potential energy (U) constant-volume thermal equilibrium fluctuations.⁴³ The degree of $W - U$ correlations is quantified by the standard Pearson coefficient given by

$$R_{WU} = \frac{\langle \Delta W \Delta U \rangle_{NVT}}{\sqrt{\langle (\Delta W)^2 \rangle_{NVT} \langle (\Delta U)^2 \rangle_{NVT}}},$$

where $\langle \dots \rangle_{NVT}$ denotes canonical ensemble averaging and $\Delta A = A - \langle A \rangle_{NVT}$ denotes statistical fluctuations around the canonical mean. Strong $W - U$ correlations are empirically delimited by the practical condition $R_{WU} \gtrsim 0.9$ that allows for straightforward identification of R-simple systems with canonical (NVT) computer simulations.

A recent computational investigation revealed that the YOCP is an R-simple system that exhibits exceptionally strong $W - U$ correlations ($R_{WU} > 0.99$) for an extended part of the fluid phase covering the entire dense liquid region of the phase diagram.⁴⁴ This rationalizes a number of previous observations such as the fact that the YOCP excess internal energies conform to the Rosenfeld-Tarazona decomposition^{45,46} and the fact that the YOCP reduced transport coefficients strongly abide to Rosenfeld's excess entropy scaling.^{47,48}

C. The isomorph-based empirically modified hypernetted-chain approximation

The *isomorph-based empirically modified hypernetted-chain (IEMHNC) approximation* is an integral equation theory approach that is based on the assumption of isomorph invariance of bridge functions when expressed in reduced distance units.²⁷ The invariance ansatz closes the non-linear non-local equation system that arises in integral equation theory provided that two external inputs are also available: a closed-form expression for the dependence of the isomorph curves on the thermodynamic state points and a closed-form bridge function expression that is valid along any phase diagram line that possesses a unique intersection point with any isomorph curve.²⁷ With such input, the isentropic correspondence maps the bridge function from the initial phase diagram line to the entire phase diagram.

The IEMHNC approach has been successfully applied to dense Yukawa and bi-Yukawa liquids^{27–29} taking advantage of an established parameterization of the OCP bridge function through the reduced distance and coupling parameter.¹⁹ Comprehensive benchmarking with computer simulations has revealed that the IEMHNC

approach possesses a remarkable accuracy with predictions of structural properties within 2% inside the first coordination cell and predictions of thermodynamic properties within 0.5% in the entire dense liquid regime.^{27,28} In addition, a systematic comparison with different advanced integral equation theory approaches has demonstrated that the performance of the IEMHNC approach is comparable to that of the variational modified hypernetted-chain (VMHNC)⁴⁹ approach but with 10–80 times less computational cost depending on the state point.²⁹

D. Theoretical arguments in favor of the isomorph invariance of bridge functions

The excellent performance of the IEMHNC approach for YOCP systems²⁷ and for biYOCP systems²⁸ clearly suggests that the underlying conjecture of the isomorph invariance of bridge functions must hold to a high degree. This is also indicated by the fact that the IEMHNC approach preserves its OCP level of accuracy regardless of the value of the YOCP or biYOCP screening parameter. Moreover, the VMHNC bridge function has been revealed to be implicitly isomorph invariant for the YOCP, since the effective packing fraction acquired by minimizing the respective free energy functional has been demonstrated to remain nearly constant along any isomorph curve within the dense liquid regime.²⁹ Finally, the output of the classic hypernetted-chain (HNC) approach, which completely neglects all the bridge diagrams, leads to approximately invariant static correlations for the YOCP,²⁷ which implies that the addition of an isomorph invariant bridge function would be beneficial for this isomorph invariance to persist.

Further arguments in support of the bridge function isomorph invariance are connected to the notion of bridge function quasi-universality⁵⁰ that forms the backbone of the powerful modified hypernetted-chain (MHNC) and reference hypernetted-chain (RHNC) approaches. This quasi-universality notion can be summarized in the statement that, in their short range, the bridge functions constitute the same universal family of curves irrespective of the interaction potential, and it was based on the fact that bridge functions can be expressed as densely connected diagrams containing total correlation function bonds.⁵⁰ Considering the isomorph invariance of the total correlation functions, the same reasoning can be extended to the notion of isomorph invariance. The isomorph theory has already rationalized a number of well-established quasi-universalities of simple liquids, since the excess entropy always turned out to be the controlling parameter.⁴¹ In addition, the isomorph invariance of bridge functions is consistent with the zero-separation bridge function freezing criterion of Rosenfeld, which states that the value of the bridge function at the origin $r = 0$, when calculated along the liquid–solid phase transition line, is nearly constant and even independent of the pair potential.⁵¹ This criterion is known to be satisfied for the YOCP.⁵²

Finally, let us discuss an apparent incompatibility of the bridge function isomorph invariance with the locality condition also known as the unique functionality condition, which assumes that the exact functional relation between the bridge function and the indirect correlation function approximately reduces to a unique function.⁵³ This condition is implicitly invoked in most fundamental bridge

function closures of integral equation theory.⁵³ However, given the isomorph variance of the indirect correlation function (to be revealed in Sec. V), it also implies that the bridge function cannot be isomorph invariant. Conversely, the approximate bridge function properties of isomorph invariance and unique functionality are incompatible. This does not constitute a contradiction, since it has been revealed (with the use of Duh–Haymet plots) that the above formulation of the locality condition does not hold over the whole range.²³ In fact, the optimized locality conditions that are invoked in more modern approaches feature a re-normalized indirect correlation function, typically stemming from a partition of the interaction potential.^{54–57} Such formulations are not incompatible with the isomorph invariance ansatz.

III. ISOMORPH TRACING AND STATE POINTS OF INTEREST

Different methods are available for the tracing of the isomorph curves of R-simple systems with or even without the use of computer simulations. In the present investigation, we shall employ the direct isomorph check, the small step method, and the analytical method. The physical basis and the numerical implementation of these methods are briefly described below.

The *direct isomorph check* is based on an approximate relation valid for any state point that is a fundamental characteristic of R-simple systems and reads as⁴²

$$U(\mathbf{R}) = U[n, S_{\text{ex}}(\tilde{\mathbf{R}})],$$

where $U(\mathbf{R})$ is the instantaneous potential energy that depends on the configuration \mathbf{R} consistent with any state point (n, T) , $S_{\text{ex}}(\tilde{\mathbf{R}})$ is the instantaneous excess entropy function that depends on the reduced configuration $\tilde{\mathbf{R}} = n^{1/3}\mathbf{R}$, and $U(n, S_{\text{ex}})$ is the thermodynamic (ensemble averaged) potential energy. Let us suppose an (n_1, T_1) reference state together with its isomorph (n_2, T_2) state of re-scaled density $n_2 = (1/\mu^3)n_1$ but unknown temperature T_2 . Let us also consider the configurations $\mathbf{R}_1, \mathbf{R}_2$ of these state points that are identical in reduced units, $n_1^{1/3}\mathbf{R}_1 = n_2^{1/3}\mathbf{R}_2$. Application of the above relation for both the state points, first-order Taylor expansion with respect to $S_{\text{ex}}(\tilde{\mathbf{R}})$ around the thermodynamic excess entropy S_{ex} , utilization of the identity $(\partial U/\partial S_{\text{ex}})_n = T$, and use of the identical reduced entropies and reduced configurations, leads to the approximate expression⁴²

$$\frac{U(\mathbf{R}_1) - U_1}{U(\mathbf{R}_2) - U_2} \approx \frac{T_1}{T_2}.$$

The above expression constitutes the basis of the direct isomorph check that in practice works as follows.^{58,59} The potential energy $U(\mathbf{R}_1)$ is extracted from an (n_1, T_1) simulation, the configuration is rescaled to $\mathbf{R}_2 = \mu\mathbf{R}_1$, and the potential energy $U(\mathbf{R}_2)$ is extracted. Repetition of this procedure for numerous \mathbf{R}_1 configurations leads to a scatter plot between $U(\mathbf{R}_1)$ and $U(\mathbf{R}_2)$ that is well approximated by a straight line and whose linear regression slope T_1/T_2 allows for the determination of the unknown T_2 .

In the present application of the direct isomorph check, the algorithm is formulated in terms of (Γ, κ) and a fixed screening parameter jump $\Delta\kappa/\kappa = 3.1\%$ is considered, which translates to a $|\Delta n|/n = 9.8\%$ density variation between successive isomorph state points. In the NVT MD simulations that are necessary for the slope extraction, reduced units are employed by setting the temperature and density equal to unity and controlling the length and energy parameters of the potential. The interaction potential is truncated at $r_{\text{cut}} = 10\Delta$ with the shifted-force cutoff method, the time step is $\Delta t/\tau = 2.5 \times 10^{-3}$, the equilibration time is $2^{20}\Delta t$, the statistics duration is $2^{20}\Delta t$, the saving period is $2^{10}\Delta t$, and the number of particles is 8192 (20Δ for the simulation box length).

The *small step method* combines the thermodynamic definition of the so-called density-scaling exponent with an exact alternative expression that originates from thermodynamic fluctuation theory. The density-scaling exponent $\gamma(n, T)$ is defined in log–log density–temperature phase diagrams as the local slope of the isentropic line traversing the state point (n, T) . Thus, we have^{38,60}

$$\gamma(n, T) = \left(\frac{\partial \ln T}{\partial \ln n} \right)_{S_{\text{ex}}},$$

with S_{ex} denoting the excess entropy. The density-scaling exponent is also acquired by the linear regression slope of the scatter plot between the virial and potential energy canonical fluctuations, since we also have^{38,60}

$$\gamma(n, T) = \frac{(\Delta U \Delta W)_{\text{NVT}}}{\langle (\Delta U)^2 \rangle_{\text{NVT}}}.$$

The fluctuation theory expression allows for the evaluation of $\gamma(n, T)$ at any state point from canonical simulations, whereas the thermodynamic definition constitutes an explicit non-linear first-order differential equation with respect to the state points that can be solved with any numerical scheme in order to trace the respective isomorph. This procedure has been coined as the small step method because its typical applications utilize first-order numerical schemes for the solution of the differential equation that necessitate small steps in the density.^{61,62} However, implementation of higher-order schemes, such as the classical fourth-order Runge–Kutta method (RK4), allows for larger density increments and leads to equally accurate isomorph tracing but with far less computational cost.

In the present application of the small step method, the RK4 algorithm is formulated in terms of $(\ln n, \ln T)$ and a fixed logarithmic density step is considered, which translates to a $|\Delta n|/n = 8.8\%$ density variation between successive isomorph state points. In the NVT MD simulations that are necessary for γ extraction, natural units (n, T) are employed, the Yukawa pair potential is truncated at $r_{\text{cut}} = 10d$ with the shifted-force cutoff method, the time step is $\Delta t/\tau = 2.5 \times 10^{-3}$, the equilibration time is $2^{17}\Delta t$, the statistics duration is $2^{17}\Delta t$, the saving period is $2^7\Delta t$, and the number of particles is 8192 ($32d$ for the simulation box length).

The *analytical method* exploits a number of exact properties of inverse power law potentials in order to define an approximate distance dependent IPL-like exponent for arbitrary pair potentials.⁶³

Complemented with a realistic estimate for the effective nearest-neighbor distance, such a definition leads to an approximate relation for the density-scaling exponent and a closed-form expression for any family of isomorphous curves.^{44,63} The application of the analytical method to YOCP systems results in⁴⁴

$$\Gamma_{\text{ISO}}(\kappa)e^{-\Lambda\alpha\kappa}\left[1 + \Lambda\alpha\kappa + \frac{1}{2}(\Lambda\alpha\kappa)^2\right] = \text{const.},$$

where Λ denotes a weakly state-point dependent parameter with a value close to unity and $\alpha = \Delta/d = (4\pi/3)^{1/3}$ denotes the ratio between the mean-cubic inter-particle distance and the Wigner-Seitz radius. The simple choice $\Lambda = 1$ has proven to be very accurate for the YOCP,⁴⁴

$$\Gamma_{\text{ISO}}(\kappa)e^{-\alpha\kappa}\left[1 + \alpha\kappa + \frac{1}{2}(\alpha\kappa)^2\right] = \text{const.} \quad (1)$$

The above expression is identical to the well-known semi-empirical description of the YOCP melting line^{64,65}

$$\Gamma_{\text{m}}(\kappa)e^{-\alpha\kappa}\left[1 + \alpha\kappa + \frac{1}{2}(\alpha\kappa)^2\right] = \Gamma_{\text{m}}^{\text{OCP}}, \quad (2)$$

which accurately follows the near-exact data obtained by MD simulations.^{66,67} In the above, $\Gamma_{\text{m}}^{\text{OCP}} = 171.8$ is the OCP coupling parameter at melting.⁶⁶ It is evident that all isomorph lines are

nearly parallel to the melting line, an observation that is true for any R-simple system to the first order.^{38,68}

In the present work, the analytical method will only be invoked in order to specify the OCP members, $\Gamma_{\text{ISO}}^{\text{OCP}}$, of YOCP isomorphs. The mapping should be very accurate, since Eqs. (1) and (2) are nearly exact for $\kappa \lesssim 1.5$. In addition, the equivalence of Eqs. (1) and (2) results in $\Gamma/\Gamma_{\text{m}} = \text{const.} \leq 1$ along any distinct isomorph. For brevity, in what follows, the constant approximate values of $\Gamma_{\text{ISO}}^{\text{OCP}}$ or Γ/Γ_{m} will be utilized in order to uniquely identify the isomorphs.

YOCP bridge functions will be determined for 16 state points that are equally spread among four different isomorphous curves. The *normalized screening parameters* κ of interest are $\kappa = (1.0, 1.5, 2.0, 2.5)$, since, for $\kappa \lesssim 1$, the YOCP behavior becomes nearly OCP-like, while, for $\kappa \gtrsim 3$, the YOCP behavior becomes nearly hard-sphere-like. Such values are typically realized in complex plasma micro-gravity experiments.^{36,69} The *OCP coupling parameters* of interest are $\Gamma_{\text{ISO}}^{\text{OCP}} = (160, 120, 80, 40)$ and span the whole dense YOCP liquid regime, since they correspond to $\Gamma/\Gamma_{\text{m}} = (0.93, 0.70, 0.47, 0.23)$, respectively. The $\kappa = 1$ members of these four isomorphs are then calculated with the analytical method, Eq. (1), which leads to $\Gamma_{\text{ISO}}^{\kappa=1} = (205.061, 153.796, 102.531, 51.265)$ that are the starting state points of the direct isomorph check and the small step method. The isomorphous coupling parameters are determined exactly using the remaining screening parameters ($\kappa = 1.5, 2.0, 2.5$) by a targeted jump from the closest κ point that emerges from the algorithms depending on their assumed density variations.

The YOCP state points of interest are listed in Table I. In all cases, the relative deviations between the results of the direct isomorph check and the small step method are always less than 0.53%.

TABLE I. $\kappa = (1.0, 1.5, 2.0, 2.5)$ members of the $\Gamma_{\text{ISO}}^{\text{OCP}} = (160, 120, 80, 40)$ or $\Gamma/\Gamma_{\text{m}} = (0.93, 0.70, 0.47, 0.23)$ isomorphs. The coupling parameters resulting from the analytical method (Γ_{ana}), direct isomorph check (Γ_{dic}), and small step method (Γ_{ssm}) are reported. The absolute relative deviations between Γ_{ana} and Γ_{dic} are denoted $e_{\text{ana/dic}}$, whereas those between Γ_{ssm} and Γ_{dic} are denoted $e_{\text{ssm/dic}}$. The correlation coefficient between virial and potential energy fluctuations R_{WU} is reported together with the density-scaling exponent γ .

κ	Γ_{ana}	Γ_{dic}	Γ_{ssm}	$e_{\text{ana/dic}}$ (%)	$e_{\text{ssm/dic}}$ (%)	R_{WU}	γ
1.0	205.061	205.061	205.061	0.00	0.00	0.990	0.522
1.5	283.178	286.437	286.289	1.14	0.05	0.990	0.712
2.0	426.757	435.572	435.268	2.02	0.07	0.994	0.939
2.5	684.511	708.517	707.487	3.39	0.14	0.996	1.192
1.0	153.796	153.796	153.796	0.00	0.00	0.991	0.523
1.5	212.383	215.930	215.542	1.64	0.18	0.992	0.715
2.0	320.068	328.816	328.710	2.66	0.03	0.994	0.938
2.5	513.384	534.722	534.034	3.99	0.13	0.995	1.189
1.0	102.531	102.531	102.531	0.00	0.00	0.988	0.529
1.5	141.589	144.330	144.325	1.90	0.00	0.991	0.720
2.0	213.378	219.972	220.496	3.00	0.24	0.992	0.940
2.5	342.256	357.136	358.051	4.17	0.26	0.995	1.178
1.0	51.265	51.265	51.265	0.00	0.00	0.988	0.534
1.5	70.794	72.537	72.748	2.40	0.29	0.988	0.730
2.0	106.689	110.707	111.094	3.63	0.35	0.990	0.934
2.5	171.128	178.269	179.217	4.01	0.53	0.993	1.166

Since the two MD implementations are characterized by the same number of particles (2^{13}) and statistically useful configurations (2^{10}), this should be a consequence of the very high virial–potential energy fluctuations $R_{WU} \geq 0.988$. These near-unity correlations imply that the starting equation of the direct isomorph check is exact, similar to the starting equation of the small step method. The YOCP state points that stem from the direct isomorph check were selected for bridge function computation. On the other hand, the absolute relative deviations between the results of the analytical method and the direct isomorph check can reach 4.17%. A consistent overestimation is observed for the analytical method above $\kappa \simeq 1.5$, as better illustrated in Fig. 1. This is rather expected because the analytical expression for the melting line, see Eq. (2), also overshoots the MD results above $\kappa \simeq 1.5$. Notice that the density-scaling exponent γ , constant for inverse power law systems, varies from 0.5 ($\kappa = 1.0$) to 1.2 ($\kappa = 2.5$) within each isomorph.

Finally, it is worth pointing out that the above isomorph tracing methods manage to identify the isentropic points of R-simple systems without ever calculating the excess entropy. Accurate theoretical determination of the excess entropy can be formidable due to the need for either thermodynamic integration or high-order correlation inclusion (see the Nettleton–Green expansion).⁷⁰ The same applies to the computational determination owing to the inefficiency of Widom test particle insertion methods at high densities.⁴⁸ For completeness, an estimate of the reduced excess entropy of each isomorph line has been attempted based on the equation of state suggested by Hamaguchi *et al.*^{66,67} This led to $(\Gamma_{\text{ISO}}^{\text{OCP}}, -s_{\text{ex}}) = \{(40, 2.02), (80, 2.87), (120, 3.49), (160, 3.99)\}$.

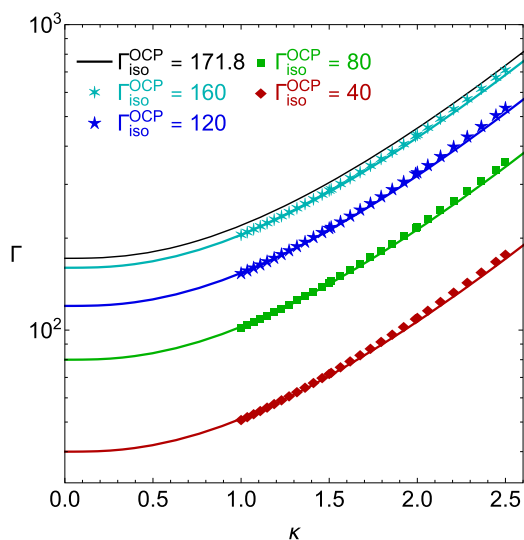


FIG. 1. Four targeted isomorphs $\Gamma_{\text{ISO}}^{\text{OCP}} = (160, 120, 80, 40)$ together with the approximate melting line $\Gamma_{\text{ISO}}^{\text{OCP}} = 171.8$ for dense YOCP liquids in the $\log \Gamma - \kappa$ phase diagram. The four isomorphic curves as obtained from the direct isomorph check (discrete symbols) are compared to those obtained from the approximate analytical expression (solid lines). The four numerical isomorphs begin to overshoot the respective analytical isomorphs roughly above $\kappa \simeq 1.5$, see also Table I.

IV. INTEGRAL EQUATION THEORY AND BRIDGE FUNCTION EXTRACTION METHODS

In the case of a one-component pair-interacting isotropic system, the integral equation theory of liquids consists of the Ornstein–Zernike (OZ) equation^{1–7}

$$h(r) = c(r) + n \int c(r')h(|r-r'|)d^3r' \quad (3)$$

and the formally exact non-linear closure condition^{1–7}

$$g(r) = \exp[-\beta u(r) + h(r) - c(r) + B(r)], \quad (4)$$

with $g(r)$ being the radial distribution function, $h(r) = g(r) - 1$ being the total correlation function, $c(r)$ being the direct correlation function, and $B(r)$ being the bridge function. Auxiliary static two-particle correlation functions of relevance are the indirect correlation function $\gamma(r) = h(r) - c(r)$, the potential of mean force $\beta w(r) = -\ln[g(r)]$, the screening potential $\beta H(r) = \beta u(r) - \beta w(r)$, and the cavity distribution function $y(r) = g(r) \exp[\beta u(r)]$. A formally exact expression for the bridge function is required to close the above system of equations.

The radial distribution function has an intuitive physical interpretation being equal to the probability density of finding a particle at a distance from a reference particle relative to the probability density for an ideal gas.⁴ The cavity distribution function also has a physical interpretation being equal to the radial distribution function for a pair of tagged particles whose mutual interaction is suppressed that are dissolved at infinite dilution in a system where all other interactions remain the same.^{1,3} The latter function remains continuous even if the interaction potential is discontinuous or diverges and acquires large but finite values near the origin $r = 0$.⁴ Finally, the potential of mean force has a physical interpretation, since the opposite of its gradient is equal to the force exerted on one member of a particle pair that is held at fixed positions, after averaging over all possible positions of the remaining particles.¹

In contrast to the radial distribution function and the cavity distribution function, the bridge function possesses neither a microscopic representation (i.e., it cannot be expressed as the ensemble average of a function that depends on the instantaneous particle positions) nor a physical interpretation (e.g., in terms of a probability density). Within the framework of diagrammatic analysis, bridge functions are graphically represented by highly connected diagrams, which contain neither nodal points nor articulation points, and their root points do not form articulation pairs. This implies that their evaluation is very cumbersome.⁵ In fact, the bridge function is formally defined through the f -bond expansion $B(r) = \sum_{i=2}^{\infty} d_i(r; T)n^i$, where the coefficients $d_i(r; T)$ are given by a number of multi-dimensional integrals whose kernels are products that involve Mayer functions $f(r) = \exp[-\beta u(r)] - 1$, or through the h -bond expansion $B(r) = \sum_{i=2}^{\infty} b_i(r; n, T)n^i$, where the coefficients $b_i(r; n, T)$ are given by a number of multi-dimensional integrals whose kernels are products that involve total correlation functions $h(r)$.^{2,71} As the order of the coefficients increases, the number of their integral constituents rises dramatically and the complexity of each kernel increases rapidly.^{72,73} More importantly, both bond expansions are known to converge very slowly already at moderate densities.^{5,71–73}

As a consequence, the direct extraction of bridge functions from computer simulations is not possible and the computation of bridge functions through their formal definition is a formidable task even with modern computational means. Nevertheless, bridge functions can be calculated with input from computer simulations by exploiting the fact that radial distribution functions, as well as cavity distribution functions, can be extracted from computer simulations and by taking advantage of the exact expressions of integral equation theory.

In the *Ornstein–Zernike inversion method*, the radial distribution function is extracted from MD or MC simulations. By inspecting Eqs. (3) and (4), it becomes evident that the bridge function acts as an additional many-body component of the pair interaction potential.⁵⁰ Hence, the computational technique utilized for the deduction of intermediate bridge functions from simulation structural data is identical to the computational method employed for the deduction of interaction potentials from experimental structural data.^{74,75} We refer to it as the OZ inversion method, since the aforementioned determination of the pair interaction potential is known as the inverse problem.⁷⁶ With knowledge of the radial distribution function, the direct correlation function is computed from the OZ equation and the bridge function is then computed from the closure condition,

$$B(r) = \ln [g(r)] - g(r) + \beta u(r) + c(r) + 1. \quad (5)$$

The extraction of radial distribution functions with the histogram method fails at short distances that lie within the so-called correlation void, where particle pair encounters are ultra-rare especially for dense systems and, thus, the collected statistics are poor even in the course of very long simulations. The correlation void can be loosely defined as $\arg_r \{g(r) \ll 1\}$ or $\arg_r \{g(r) \approx 0\}$, and its exact range depends on the thermodynamic state point of interest, see Fig. 2(a) for an illustration. For the YOCP simulations reported herein, the correlation void roughly corresponds to $r \lesssim 1.4d$. From the structure of the OZ equation, it is straightforward to deduce that the direct correlation function is insensitive to the exact small values of the radial distribution function inside the correlation void. Therefore, the direct correlation function can be accurately computed along the whole range with the OZ inversion method. On the other hand, owing to the presence of the $\ln[g(r)]$ term in the closure condition, it is evident that the bridge function is very sensitive to the exact small value of the radial distribution function inside the correlation void. Therefore, the bridge function can only be reliably computed in the intermediate and long ranges, i.e., outside the correlation void, with the OZ inversion method. In the implementation of the OZ inversion method, the main challenge turns out to be the acquisition of large statistical samples, since the bridge function in the intermediate and long ranges has a very strong sensitivity to the radial distribution function.

In the *cavity distribution method*, the cavity distribution function is directly extracted from MD or MC simulations. With knowledge of the direct correlation function from the OZ inversion method, the bridge function is then computed from the closure condition that, within the correlation void $g(r) \approx 0$, reads

$$B(r) \approx \ln [y(r)] + c(r) + 1. \quad (6)$$

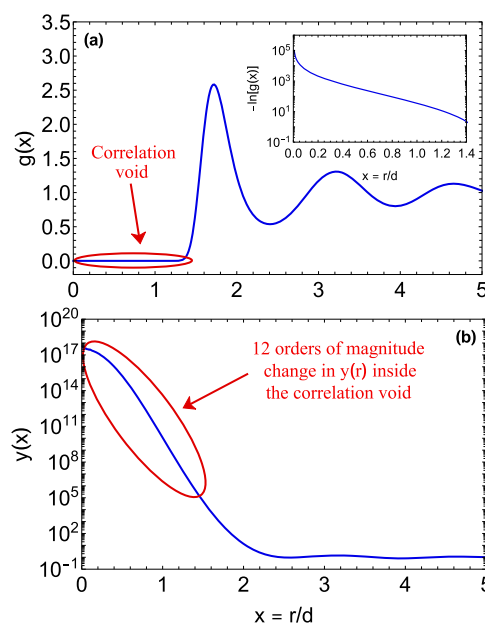


FIG. 2. Characteristics of the radial distribution function (a) and the cavity distribution function (b) for dense simple liquids. MD results for the YOCP state point $\Gamma = 708.517$, $\kappa = 2.5$ ($\Gamma_{\text{ISO}}^{\text{OCP}} = 160$). The correlation void, $\arg_r \{g(r) \approx 0\}$, is accompanied by a rapid drop in the pair particle statistics (see the inset) and a rapid increase in the cavity statistics. However, the cavity statistics are strongly non-uniform at short distances, as confirmed by the 12 orders of magnitude difference between the cavity distribution function values at the edge of the correlation void, $r \lesssim 1.4d$, and at the origin, $r = 0$.

As illustrated in Fig. 2(b), the cavity distribution function acquires very high values within the correlation void, which suggests that large global sample statistics can be obtained. However, the values of the cavity distribution function increase by many orders of magnitude from the edge of the correlation void up to the origin $r = 0$, which implies that uniform sample statistics are rather impossible to acquire owing to the fact that the very localized sub-interval close to $r = 0$ will always be over-sampled. Thus, a type of umbrella sampling technique needs to be followed that inserts a known bias, which homogenizes the statistics within the entire correlation void. This turns out to be the main challenge in the implementation of the cavity distribution method. Finally, we emphasize that the cavity distribution method needs to be complemented with the OZ inversion method for the computation of the bridge function due to the presence of the direct correlation function in the closure equation.

V. INDIRECT BRIDGE FUNCTION EXTRACTION WITH THE ORNSTEIN-ZERNIKE INVERSION METHOD

Here, the OZ inversion method will be described, the parameters of the production runs or test simulations will be provided, and the numerical results will be analyzed.

A. The computational method

In all integral equation theory approaches, Eqs. (3) and (4) are solved for $[g(r), c(r)]$ with known $u(r)$ and an assumption for $B(r)$, which suggests that the equations are coupled. In pair interaction reconstruction, Eqs. (3) and (4) are solved for $[c(r), u(r)]$ with known $g(r)$ and an assumption for $B(r)$, which suggests that multiple viable solutions can emerge. In bridge function reconstruction, Eqs. (3) and (4) are solved for $[c(r), B(r)]$ with known $[g(r), u(r)]$, which suggests that the equations are decoupled and a unique solution exists.

The computation of bridge functions with the OZ inversion method and input from standard NVT MD simulations proceeds in the following manner. (1) The radial distribution function is extracted from MD simulations using the histogram method with bins of constant width $\Delta r/d$. (2) The Fourier transform of the total correlation function is calculated. Invoking the spherical symmetry, $H(k) = (4\pi/k) \int_0^\infty [rh(r) \sin(kr)] dr$ emerges leading to $H(k_i) = (4\pi\Delta r/k_i) \sum_{j=1}^W r_j h(r_j) \sin[(\pi/W)(j - \frac{1}{2})i]$ for the discrete sine transform of a space resolution equal to the bin width (to avoid interpolations). In the above, W is the histogram bin number, $\Delta k = \pi/(N\Delta r)$, $k_i = i\Delta k$, $r_j = j\Delta r - \Delta r/2$, $r = \{r_i\}$, and $k = \{k_i\}$. Fast Fourier Transform (FFT) algorithms are employed in order to reduce the computational cost. (3) The Fourier transform of the direct correlation function is computed. By Fourier transforming the OZ equation and solving for $C(k)$, we obtain $C(k) = H(k)/[1 + nH(k)]$. (4) The direct correlation function is calculated from the inverse Fourier transform. Invoking the spherical symmetry, we obtain the expression $c(r) = [1/(2\pi^2 r)] \int_0^\infty [kC(k) \sin(kr) dk]$ that ultimately leads to the discrete inverse sine transform $c(r_i) = [\Delta k/(2\pi^2 r_i)] \{ \sum_{j=1}^{W-1} k_j C(k_j) \sin[(\pi/W)j(i - \frac{1}{2})] + R_{W,i} \}$ with $R_{W,i} = [(-1)^{i-1}/2] k_W C(k_W)$ for the residue. FFT algorithms are again employed. (5) The bridge function is computed from Eq. (5).

We re-iterate that, inside the correlation void, particle encounters are extremely rare, but their probability remains finite. As a result, the histogram method could, for instance, lead to either $g(r) = 10^{-8}$ or $g(r) = 10^{-12}$ due to the poor statistical sampling. This uncertainty does not affect the direct correlation function, but it strongly impacts the bridge function courtesy of the logarithm of the radial distribution function that is present in the OZ closure equation, leading to a significant -8 or -12 contribution for this example. In conclusion, the unavoidable insufficient statistics within the correlation void suggest that the OZ inversion method is only effective for the computation of the bridge function at intermediate and long ranges. For a given interaction potential, the validity limit mainly depends on the state point of interest, the overall statistics (number of particles and number of uncorrelated configurations), and the desired accuracy.

B. The numerical implementation

The production runs for the extraction of the radial distribution functions, as well as the tracing of the isomorph curves, were carried out on graphics cards with the RUMD open-source software.⁷⁷ A small number of test runs were performed with the LAMMPS package.⁷⁸

In the production runs that are dedicated to the $g(r)$ extraction, the NVT MD simulations utilize the shifted-force cutoff method

with the Yukawa pair potential truncated at $r_{\text{cut}} = 10d$, and the time step employed for the propagation of equations of motion is $\Delta t/\tau = 2.5 \times 10^{-3}$. The MD equilibration time is $\tau_{\text{eq}}/\Delta t = 2^{20}$, the statistics duration is $\tau_{\text{stat}}/\Delta t = 2^{23}$, and the configuration saving period is $T_{\text{save}}/\Delta t = 2^7$ leading to $M = 2^{16} (= 65\,536)$ for the number of statistically independent configurations. The particle number is $N = 54\,872$ leading to $L = 60d$ for the cubic simulation box length, and the bin width size of the histogram method is $\Delta r/d = 0.002d$. We shall refer to these production runs as ultra-accurate standard MD simulations.

The configuration saving period was selected so that uncorrelated radial distribution functions are always extracted. The combination of statistics duration and number of particles was selected so that sufficient pair correlation sample sizes are collected even up to $r = 1.25d$. The size of the histogram bin width was selected so that the grid errors are much smaller than the statistical errors. A large number of test runs were carried out in order to choose a near-optimal cutoff method, truncation radius, and MD time step. The test runs were carried out at the YOCP state point $\Gamma_{\text{ISO}}^{\text{OCP}} = 160$, $\kappa = 1.0$ for which the bridge function exhibits the highest sensitivity to uncertainties in the radial distribution function. Finally, some test runs were performed with the RUMD and the LAMMPS software for the same YOCP state points and for identical simulation settings as a validation check.

C. The numerical results

The sequential output of the OZ inversion method, i.e., $g(r) \rightarrow c(r) \rightarrow B(r)$, is illustrated in Fig. 3 for the 4 isomorph curves and 16 YOCP state points of interest. We point out that the comprehensive analysis of uncertainty propagation in the OZ inversion method, which led to the determination of the bridge function error bar levels, is detailed in Sec. II of the [supplementary material](#).

The radial distribution functions $g(r/d)$ along each isomorph are illustrated in the left panel within the interval $r/d \leq 6$, see Figs. 3(a), 3(d), 3(g), and 3(j). In addition, the potentials of mean force $-\ln[g(r)]$ are plotted within the range $1.25 \leq r/d \leq 2$ in the respective insets. As demonstrated from earlier investigations of the YOCP,⁴⁴ the radial distribution function is a strongly invariant quantity along any isomorph line except from a very narrow interval centered around the first maximum. The invariance holds to a very good approximation outside the correlation void, but it is rapidly distorted at short distances. The local variance becomes especially apparent when inspecting the potentials of mean force for $r/d \lesssim 1.5$. To be more concrete, the $g(r)$ deviations between isomorph state points reach two orders of magnitude at $r = 1.25d$ for $\Gamma_{\text{ISO}}^{\text{OCP}} = 160$ and this trend is expected to get further augmented at shorter distances. This behavior does not contradict the basic property of R-simple systems, which states that they possess approximate invariant structural properties in reduced r/d units, because it manifests itself at short distances where the radial distribution function can be approximated with zero and its exact infinitesimal values are inconsequential. In other words, this behavior concerns ultra-rare structural configurations that are physically insignificant. It is worth pointing out that the observed $g(r)$ variance within the correlation void can be deduced by inspecting the asymptotic limit of Widom's theorem, which reads as $g(r \rightarrow 0) \propto \exp[-\beta u(r)]$.⁷⁹

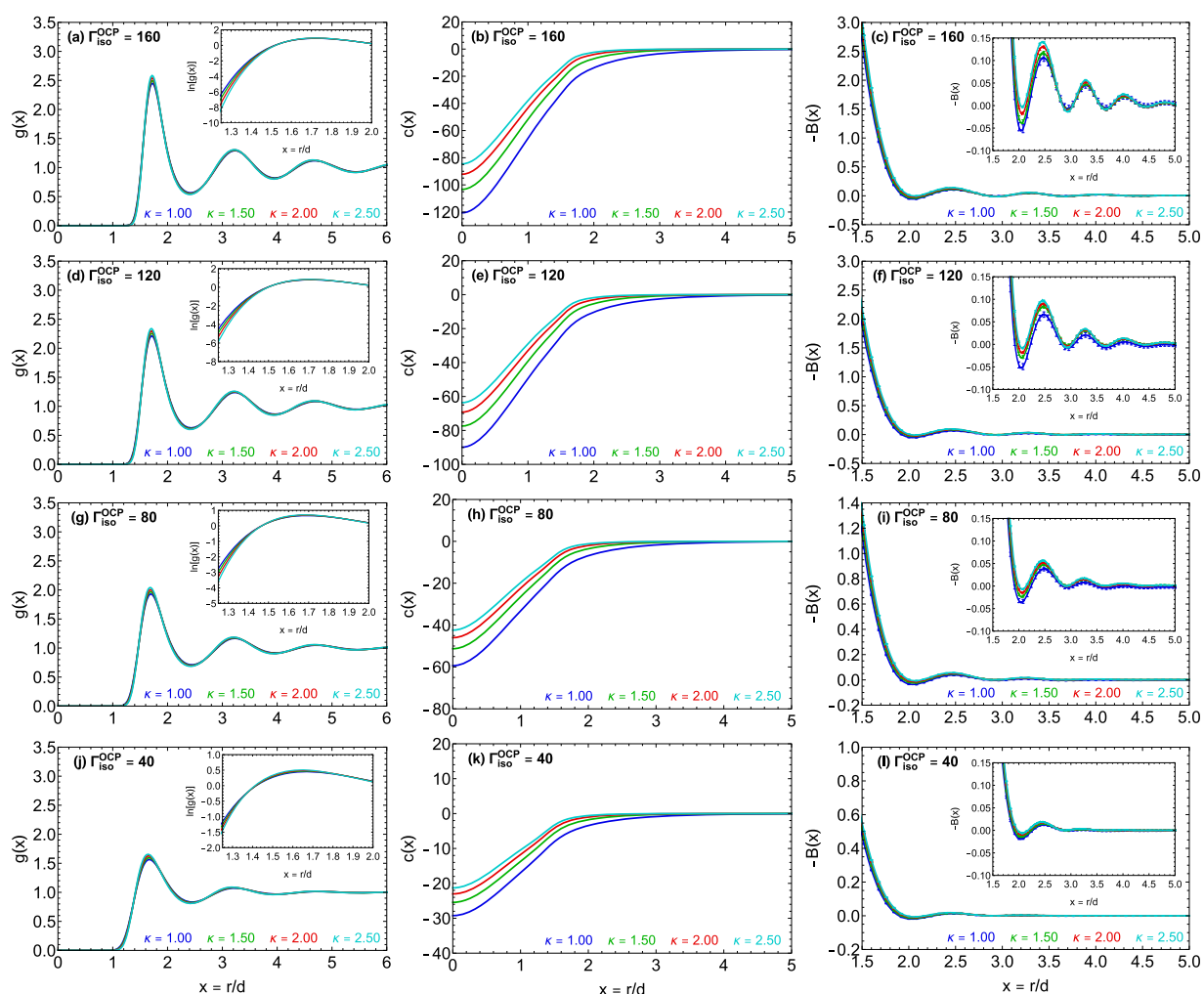


FIG. 3. Static correlation functions as computed with the OZ inversion method with input from ultra-accurate standard MD simulations. Results for the 16 YOCP state points of interest. (a), (d), (g), (j) Radial distribution function and potential of mean force for the four members of the $\Gamma_{\text{ISO}}^{\text{OCP}} = 160, 120, 80, 40$ isomorphs, respectively. (b), (e), (h), (k) Direct correlation function for the four members of the $\Gamma_{\text{ISO}}^{\text{OCP}} = 160, 120, 80, 40$ isomorphs, respectively. (c), (f), (i), (l) Bridge function including error bars for the four members of the $\Gamma_{\text{ISO}}^{\text{OCP}} = 160, 120, 80, 40$ isomorphs, respectively. The isomorph deviations and the error bars are small and can be better discerned in the zoomed-in insets. The same applies to the quasi-periodic sign switching of the bridge functions.

The direct correlation functions $c(r/d)$ along each isomorph are illustrated in the middle panel for the interval $r/d \leq 5$, see Figs. 3(b), 3(e), 3(h), and 3(k). It is evident that the direct correlation function is a strongly variant quantity everywhere. This could be expected from the reduced excess inverse isothermal compressibility relation $\bar{\mu}_T = -n \int c(r) d^3r$ and the fact that $\bar{\mu}_T$ is variant as a thermodynamic quantity that involves second order volume derivatives,⁵⁹ as well as from the exact asymptotic limit $c(r \rightarrow \infty) = -\beta u(r)$.¹⁻⁴ It is worth noting that direct correlation functions reach their asymptotic limit much faster than other static correlation functions. This takes place prior to $r/d = 2$, close to the foot of the $c(r)$ curve where the slope exhibits a rapid change. This observation justifies the

satisfactory performance of the soft mean spherical approximation for the YOCP.^{80,81}

The bridge functions $B(r/d)$, together with error bars, along each isomorph are illustrated in the right panel for the interval $1.5 \leq r/d \leq 5$, see Figs. 3(c), 3(f), 3(i), and 3(l). The insets feature a magnification of the oscillatory pattern and the small uncertainty levels of the bridge functions. It is evident that the bridge function is a strongly invariant quantity along any isomorph line in the whole range across which it can be accurately computed with the OZ inversion method. In contrast to radial distribution functions for which there are strong variant features within the correlation void and for which longer range weak variant features are

concentrated in the first maximum vicinity, the bridge function variant features appear to be uniformly spread in the whole computation range. In the long range, the observed invariance is justified by the analytic asymptotic behavior of the bridge function. Substituting for $c(r) \simeq -\beta u(r)$ and $g(r) = h(r) + 1$ in the closure equation, we have $B(r) = \ln[h(r) + 1] - h(r)$. Taylor expanding the logarithm with respect to $h(r) \simeq 0$ and retaining up to the second order term, we end up with $B(r) = -[h^2(r)]/2$. In the intermediate range, the observed invariance is in accordance with the h-bond expansion that formally defines the bridge function through the infinite series $B(r) = \sum_{i=2}^{\infty} b_i [h(r)] n^i$, where the unknown weighting functions are given by multiple integrals that solely involve the total correlation function.^{2,71} Since the integration space for the weighting function of the n^i term is \mathbb{R}^{3i} , the introduction of reduced units r/d or r/Δ means that all the powers of the density vanish for each term, thus leading to $B(r/d) = \sum_{i=2}^{\infty} b_i [h(r/d)]$, which suggests that a $h(r/d)$ isomorph invariance implies a $B(r/d)$ isomorph invariance.

It is evident that uncertainties cannot account for the small deviations observed between the bridge functions of the different members of the same isomorph. Therefore, the observed isomorph invariance of bridge functions in the long and intermediate ranges $r \geq 1.5d$ is only approximate. Notice that the relative invariance holds to nearly the same degree regardless of the YOCP isomorph. Note also that the approximate bridge function invariance extends up to the edges of the correlation void, where the approximate radial distribution function invariance begins to break down. Finally, it is worth pointing out that, for all the 16 YOCP state points investigated, the bridge function becomes slightly positive close to $r \simeq 2d$ well within the recorded uncertainties. In rough accordance with the asymptotic behavior of $B(r) = -(1/2)h^2(r)$ and with the $\sim 1.5d$ periodicity of the total correlation function, additional shallower positive maxima appear with a periodicity slightly less than $\sim 0.8d$. The emergence of the sign switching and positive maximum within the first coordination cell seems to be a standard characteristic of bridge functions of dense simple fluids that has also been observed for hard-sphere systems,¹⁰ Lennard-Jones liquids,^{12,13} IPL-12 systems,¹⁶ and OCP liquids.¹⁹ It is a salient feature of bridge functions that cannot be captured by the VMHNC approximation⁴⁹ that utilizes the non-positive analytical Percus–Yevick hard-sphere bridge function. This deficiency has been suggested as responsible for the minor structural inaccuracies of the VMHNC approach that are mainly observed in the vicinity of the first peak of the YOCP radial distribution function.²⁹

VI. INDIRECT BRIDGE FUNCTION EXTRACTION WITH THE CAVITY DISTRIBUTION METHOD

A. The computational method

In the cavity simulations, two tagged particles are interacting with a specially designed pair potential that allows them to explore all the nearly forbidden distances within the correlation void. The potential of mean force that is exerted on the tagged particles still originates from the remaining $N - 2$ particles. The tagged pair potential adds an externally controlled bias that allows for the sampling of the ultra-rare pair configurations within the correlation

void. The known statistical bias can then be removed, so that the statistical weights that correspond to the actual static correlations are ultimately extracted. The cavity simulation method was originally developed by Torrie and Patey⁸ for hard-sphere potentials and non-interacting tagged particles and later generalized by Llano-Restrepo and Chapman¹² to arbitrary interaction potentials and arbitrary tagged pair potentials.

The *targeted system* is a one-component liquid that consists of N particles that interact with the pair potential $u(r)$. The *simulated system* is a binary liquid mixture that consists of $N - 2$ type A particles that interact with the potential $u(r)$ and two type B particles (tagged as 1,2) that interact with the potential $u(r)$ with type A particles, but with the potential $\psi(r)$ with each other. This system's correlation functions are denoted with the script "sim." The total potential energies of these systems are connected via $U_{\text{sim}}(\mathbf{R}) = U(\mathbf{R}) + \psi(\mathbf{r}_1, \mathbf{r}_2) - u(\mathbf{r}_1, \mathbf{r}_2)$. In the canonical ensemble, the reduced two-particle density in the targeted system and reduced two-particle density of the tagged particles in the simulated system read as

$$n_2(\mathbf{r}_1, \mathbf{r}_2) = N(N-1) \frac{\int \exp[-\beta U(\mathbf{R})] d^3 r_3 \dots d^3 r_N}{\int \exp[-\beta U(\mathbf{R})] d^3 r_1 \dots d^3 r_N},$$

$$n_2^{\text{sim}}(\mathbf{r}_1, \mathbf{r}_2) = 2 \frac{\int_{V_c} \exp[-\beta U_{\text{sim}}(\mathbf{R})] d^3 r_3 \dots d^3 r_N}{\int_{V_c} \exp[-\beta U_{\text{sim}}(\mathbf{R})] d^3 r_1 \dots d^3 r_N}.$$

The constraint volume V_c in the configuration integral of the simulated system originates from the fact that the tagged particles are not allowed to explore the whole configuration space in order to enhance the statistics. The numerical pre-factors stem from particle indistinguishability and from integrand symmetry with respect to particle label interchange. Combining the above, we acquire

$$\frac{n_2^{\text{sim}}(\mathbf{r}_1, \mathbf{r}_2)}{n_2(\mathbf{r}_1, \mathbf{r}_2)} = \frac{e^{-\beta \psi(\mathbf{r}_1, \mathbf{r}_2)}}{e^{-\beta u(\mathbf{r}_1, \mathbf{r}_2)}} \frac{2 \int e^{-\beta U(\mathbf{R})} d^3 r^N}{N(N-1) \int_{V_c} e^{-\beta U_{\text{sim}}(\mathbf{R})} d^3 r^N},$$

where we introduced the notation $d^3 r_1 \dots d^3 r_N = d^3 r^N$ for brevity. We point out that the second factor is independent of the tagged particle positions $\mathbf{r}_1, \mathbf{r}_2$. In case the constraint volume V_c is smaller than the primary simulation cell volume, this factor cannot be evaluated in the course of the simulation.¹² In what follows, it will be denoted $1/C$. By introducing the radial distribution functions of both systems $g(\mathbf{r}_1, \mathbf{r}_2) = n_2(\mathbf{r}_1, \mathbf{r}_2)/n^2$, exploiting the isotropy of the interaction potentials, and introducing the cavity distribution function of the targeted system $y(r_{12}) = g(r_{12}) \exp[\beta u(r_{12})]$ with $r_{12} = |\mathbf{r}_1 - \mathbf{r}_2|$, we finally obtain

$$y(r) = C \exp[\beta \psi(r)] g_{\text{sim}}^{12}(r) \quad (7)$$

after setting $r = r_{12}$ and $g_{\text{sim}}^{12}(r) = g_{\text{sim}}(r_{12})$ in order to emphasize that the pair correlations of tagged particles should be sampled. Owing to the continuity of the cavity distribution function, the unknown constant C should be determined by matching with known $y(r)$ values either outside the correlation void (obtained by OZ inversion) or at

the origin (obtained by Widom's expansion⁷⁹). The former option is generally preferable being accompanied by smaller statistical errors.

Overall, in cavity simulations, the radial distribution function of the two tagged particles $g_{\text{sim}}^{12}(r)$ is extracted with the histogram method, which leads to the determination of the short range distance dependence of the cavity distribution function $y(r)$ of the targeted system, see Eq. (7). The unknown proportionality constant C is then quantified by a matching procedure with available intermediate range $y(r)$ results at the upper edge of the correlation void, which leads to the determination of the short range cavity distribution function $y(r)$ of the real system, see Eq. (7) again. Finally, the short range bridge function $B(r)$ can be determined from Eq. (6) with knowledge of the short range $\ln[y(r)]$ and the full range $c(r)$, the latter reliably obtained from the OZ inversion method. The main difficulties in the cavity simulation method are connected with the specification of the tagged pair potential $\psi(r)$. In fact, as we shall describe in what follows, multiple preliminary cavity simulations will be required in order to make an informed guess for $\psi(r)$ that is accurate enough for reliable bridge functions to be computed.

The tagged pair potential $\psi(r)$ should ensure that the entire correlation void is sampled as uniformly as possible by the tagged particle pair. Otherwise, large statistical errors will emerge in the poorly sampled annular rings. It is evident that the tagged pair potential $\psi(r)$ should strongly depend on the thermodynamic state point. The acquisition of uniform statistics along the correlation void is a complicated task, since it requires an accurate guess of the potential of mean force $-\ln[g(r)]$ that, in turn, requires an accurate guess of the short range bridge function $B(r)$ that is our unknown. It is far more practical to separate the correlation void into a number of successive overlapping windows ($I_n = [b_n, c_n]$ with $c_n > b_{n+1}$) by imposing hard constraints in the tagged particle motion. In fact, the potentials of mean force can be guessed more accurately with an iterative computational scheme at shorter intervals wherein the relative variations in $g(r)$ are far less dramatic, while the overlap is required in order to determine the unknown proportionality constant C of Eq. (7) by means of sequential matching.^{21,26} On the other hand, the hard constraints can also be viewed as flexible bond lengths and be implemented through the tagged pair potential itself.¹³ Overall, the tagged pair potential $\psi(r)$ is decomposed into a windowing component $\chi(r)$ that confines the tagged particles within given finite intervals and a biasing component $\phi(r)$ that uniformly samples each windowing interval, i.e.,

$$\psi_n(r) = \chi_n(r) + \phi_n(r), \quad (8)$$

where n is the number of successive overlapping windows.

It is preferable that the *windowing component* of the tagged pair potential does not affect the correlation sampling within each window, implying that $d\chi(r_n)/dr \approx 0$, $\forall r_n \in I_n$. It is also essential that the windowing component is steep enough at the vicinity of each window's edges, so that the tagged particles cannot traverse the restriction zone even in the course of long simulations. An infinite potential well appears to be the most straightforward mathematical implementation. Due to the involvement of infinities, the practical implementation is quite involved, since it becomes necessary to

treat impulsive elastic collisions. As a result, the smooth finite potential well that is generated by the sum of two error functions was preferred. In normalized units $\beta\chi(x)$ with $x = r/d$,

$$\beta\chi_n(x) = a_1 \{ \text{erf}[a_2(a_{3n} - x)] + \text{erf}[a_2(a_{4n} - x)] \}, \quad (9)$$

where the state variable dependent coefficient $a_1(n, T)$ controls the well depth, the constant coefficient a_2 controls the well steepness, and the window dependent coefficients (a_{3n}, a_{4n}) control the well extent and position. The coefficients (a_2, a_{3n}, a_{4n}) should be selected such that $\chi(x) \approx \text{constant}$ within each window, while the coefficients (a_1, a_2) should be selected such that tagged particles do not escape the windowing interval. It is worth noting that very steep realizations might turn out to be problematic and counter-intuitively lead to loss of tagged particle confinement due to the insufficient MD time steps. After a consideration of the above rough guidelines, the exact coefficients should be determined by trial and error.

In each window, the *biasing component* of the tagged pair potential, which should counteract the absent pair repulsion and the potential of mean force, is initially determined through a series of short cavity simulations with the following iterative procedure, which is based on Eq. (7) and the multiplicative identity of exponentials: (a) The tagged particles are assumed to be non-interacting, a cavity simulation is performed, $g_{\text{sim}}^{12}(x)$ is extracted, and its logarithm is interpolated with a Gaussian function $G_1(x)$. (b) The biasing component is assumed to be given by $\beta\phi(x) = G_1(x)$, another cavity simulation is performed, $g_{\text{sim}}^{12}(x)$ is extracted, and its logarithm is interpolated with a Gaussian function $G_2(x)$. (c) The biasing component is then assumed to be given by $\beta\phi(x) = G_1(x) + G_2(x)$, and the procedure is repeated resulting in an additional Gaussian function. (d) The iterative procedure is terminated, when the targeted interval is judged to be sufficiently sampled. In this manner, the biasing component is approximated by a series of Gaussian functions, i.e.,

$$\beta\phi_n(x) = \sum_{i=1}^k d_{1,i,n} \exp[-d_{2,i,n}(x - d_{3,i,n})^2], \quad (10)$$

where k is the number of iterations and the coefficients ($d_{1,i,n}, d_{2,i,n}, d_{3,i,n}$) are determined by least square fits. The iteration scheme proved to be robust and leads to analytical approximations for the biasing potential. Its major disadvantage is concerned with the fact that $\beta\phi_n(x)$ is not necessarily monotonic, which can lead to tagged particle trapping in the course of very long simulations. Such trapping would cause non-uniform sampling and induce spurious correlations between samples collected at different time steps, generating uncertainties that would be hard to quantify. The following remedy proved to be successful: (a) Long MD cavity simulations are performed at each interval using Eqs. (8)–(10), the sub-interval cavity distribution functions are matched, and the cavity distribution function $y(r)$ is extracted along the entire domain. (b) From Widom's cavity distribution function expansion,⁷⁹ it is expected that the short range cavity logarithm can be well approximated by an even polynomial, $\ln[y(r)] = \sum_{i=0}^l y_{2i} r^{2i}$. Least square fitting confirmed that this expansion is very accurate and led to the determination of the coefficients y_{2i} . Note that $\ln[y(r)]$ is now monotonic. (c) Given that

$\ln[g(r)] = \ln[y(r)] - \beta u(r)$, it is evident that the improved biasing component becomes $\beta\phi(r) = \ln[y(r)]$ or equivalently

$$\beta\phi(x) = \sum_{i=0}^l y_{2i} x^{2i}, \quad (11)$$

where l is the minimum number of polynomial terms that ensures an excellent fit to the short range $\ln[y(r)]$ data. This expression for the biasing component of the tagged pair potential is valid in the entire short range of interest. However, this does not suggest that the windowing technique should be abandoned in the final ultra-long cavity simulations, since a broader windowing is still essential to confine the tagged particles within the correlation void.

B. The numerical implementation

The NVT MD simulations for the cavity distribution function extraction in the short range were carried out on graphics cards with the RUMD open-source software.⁷⁷ The shifted-force cutoff method is used with $r_{\text{cut}}/d = 8$, $\Delta t/\tau = 2.5 \times 10^{-3}$, $\tau_{\text{eq}}/\Delta t = 2^{19}$, $T_{\text{save}}/\Delta t = 2^7$, $N = 1000$ (998 type A particles and 2 type B particles), $L/d \simeq 16$, and $\Delta r/d = 0.002$. The statistics duration and, thus, the statistically independent configuration number varied strongly, depending on the simulation type. Four overlapping windows are used for the tagged pair, namely (in r/d units), $I_1 = [0.0, 0.4]$, $I_2 = [0.2, 0.6]$, $I_3 = [0.4, 1.0]$, and $I_4 = [0.8, 1.4]$, while we have $I_5 = [1.25, \infty)$ for the results that are available from the OZ inversion method.

It is important to justify the relatively low simulated particle number ($N = 1000$). In the cavity simulations, the radial distribution function $g_{\text{sim}}^{12}(r)$ of the two tagged particles is extracted. Consequently, a single correlation event is recorded per statistically independent configuration rather than the $N(N-1)/2$ correlation events per configuration that are recorded during the extraction of the radial distribution function $g(r)$ of the targeted system. Since the statistical sample cannot be increased by simulating a larger number of particles, N should be kept as low as possible in order to reduce the computational cost. Nevertheless, in case of very low particle numbers, finite size effects inevitably begin to affect the short range static correlations. The conservative $N = 1000$ choice ensures that such errors are negligible. A thorough study of the N -dependence of the cavity distribution functions is reported in Sec. III of the [supplementary material](#).

In the *short cavity simulations*, dedicated to the determination of the unknown coefficients of the windowing component and of the Gaussian representation of the biasing component, Eqs. (9) and (10), we have $\tau_{\text{stat}}/\Delta t = 2^{19}$ and $M_1 = 2^{12}$ for the statistically independent configuration number. For an arbitrary interval $I_n = [b_n, c_n]$, the windowing coefficients were found to be $a_1(\Gamma, \kappa) = (25-360)$ depending on the state point, $a_2 = 20$ regardless of the state or confinement interval, $a_{3n} = b_n - 0.1$, and $a_{4n} = c_n + 0.1$. Up to three iterations sufficed to obtain a Gaussian series representation of the biasing component that allows for the relatively uniform sampling of any windowing interval. [Figure 4](#) demonstrates how tagged pair statistics become more uniform as the iterative procedure progresses.

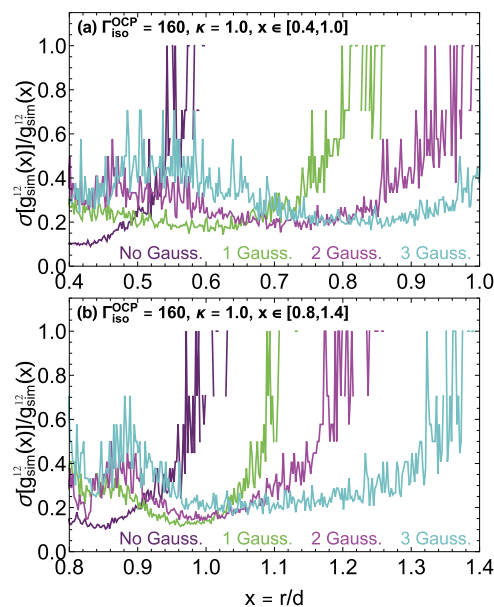


FIG. 4. Relative standard errors $\sigma[g_{\text{sim}}^{12}(r)]/g_{\text{sim}}^{12}(r)$ in the extraction of the radial distribution function of the two tagged particles $g_{\text{sim}}^{12}(r)$ from *short cavity simulations* for different biasing components of the tagged pair potential. Results for the YOCP state point $\Gamma_{\text{ISO}}^{\text{OCP}} = 160$, $\kappa = 1.0$ in the windowing intervals (a) $I_3 = [0.4, 1.0]$ and (b) $I_4 = [0.8, 1.4]$. In both cases, as the iterative procedure progresses and the biasing component $\beta\phi_n(x)$ is refined by the addition of successive Gaussian functions, $\sigma[g_{\text{sim}}^{12}(r)]/g_{\text{sim}}^{12}(r)$ gradually becomes more uniform in the respective windowing interval. Given the small $M_1 = 2^{12}$ sample size, the $\sigma[g_{\text{sim}}^{12}(r)]/g_{\text{sim}}^{12}(r) \sim 0.3$ level is too high for reliable computation of short range bridge functions but will be greatly reduced in the long and ultra-long cavity simulations.

In the *long cavity simulations*, dedicated to the determination of the unknown coefficients of the Widom polynomial representation of the biasing component, Eq. (11), we have $\tau_{\text{stat}}/\Delta t = 2^{27}$ and $M_2 = 2^{20}$. The matching procedure, which was followed in the overlapping extent of consecutive windows starting from $I_5 \cap I_4$ and proceeding up to $I_2 \cap I_1$, led to very accurate proportionality constants C_i that are documented in [Table II](#). Note that due to the extremely large cavity values that emerge in the correlation void, it is preferable to work with natural logarithms. This transforms Eq. (7) into $\ln[y(r)/y_{\text{sim}}(r)] = \ln C$ with $y_{\text{sim}}(r) = g_{\text{sim}}^{12}(r) \exp[\beta\psi(r)]$. Least square fitting for the cavity logarithm $\ln[y(r)]$ revealed that the first three terms of the Widom expansion suffice for a very accurate representation in the short range. In particular, the absolute relative errors were always less than 0.53%. The polynomial coefficients y_0, y_2, y_4 are reported in [Table III](#). As illustrated in [Fig. 5](#), the Widom expansion is valid within the entire correlation void and will be ultimately utilized in the final cavity simulations.

In the *ultra-long cavity simulations*, dedicated to the accurate determination of the cavity distribution function in the short range, we have $\tau_{\text{stat}}/\Delta t = 2^{32}$ and $M_3 = 2^{25}$. The windowing component of the tagged pair potential now confines the type B particles within the correlation void $I = [0.0, 1.4]$. The windowing coefficients were

TABLE II. Results of the long cavity simulation matching procedure for all the 16 YOCP state points of interest. Matching in the overlapping interval $I_5 \cap I_4 = [1.25, 1.4]$ leads to the constant $\ln C_4$, matching in the overlapping interval $I_4 \cap I_3 = [0.8, 1.0]$ leads to the constant $\ln C_3$, matching in the overlapping interval $I_3 \cap I_2 = [0.4, 0.6]$ leads to the constant $\ln C_2$, and matching in the overlapping interval $I_2 \cap I_1 = [0.2, 0.4]$ leads to the constant $\ln C_1$. In each matching stage, the *a priori* knowledge of the logarithm of the cavity distribution function in the outer interval allows for its determination in the inner interval, starting from the intermediate and the long range region I_5 where $\ln[y(r)]$ is known from the Ornstein–Zernike inversion method. In particular, the proportionality constant is determined by least square fitting $\ln[y_{I_n}(r)/y_{\text{sim}}(r)] = \ln C_{n-1} \forall r \in I_n \cap I_{n-1}$, which allows for the determination of $y_{I_{n-1}}(r)$ from $\ln[y_{I_{n-1}}(r)/y_{\text{sim}}(r)] = \ln C_{n-1} \forall r \in I_{n-1}$. The extremely low mean absolute relative deviations $e_{\ln C_n} (< 0.04\%)$ confirm the theoretical expectation that the ratio $\ln[y(r)/y_{\text{sim}}(r)]$ is well-approximated by a constant.

$\Gamma_{\text{ISO}}^{\text{OCP}}$	κ	Γ	$\ln C_4$	$e_{\ln C_4} (\%)$	$\ln C_3$	$e_{\ln C_3} (\%)$	$\ln C_2$	$e_{\ln C_2} (\%)$	$\ln C_1$	$e_{\ln C_1} (\%)$
160	1.0	205.061	235.730	0.012	244.758	0.042	261.285	0.010	261.440	0.006
160	1.5	286.437	302.777	0.012	316.536	0.008	325.572	0.006	325.385	0.006
160	2.0	435.572	441.541	0.003	455.055	0.005	463.919	0.005	463.091	0.005
160	2.5	708.517	715.668	0.002	728.484	0.005	729.232	0.003	728.703	0.002
120	1.0	153.796	170.868	0.009	183.632	0.012	192.335	0.012	191.752	0.010
120	1.5	215.930	227.321	0.008	233.451	0.009	241.817	0.010	240.948	0.008
120	2.0	328.816	302.777	0.012	316.536	0.008	325.572	0.006	325.385	0.006
120	2.5	534.722	535.023	0.002	539.746	0.003	546.893	0.005	545.983	0.004
80	1.0	102.531	111.524	0.012	115.741	0.018	122.975	0.019	121.844	0.017
80	1.5	144.330	146.383	0.009	149.329	0.015	156.405	0.016	155.272	0.012
80	2.0	219.972	224.016	0.007	227.331	0.009	226.880	0.009	225.569	0.010
80	2.5	357.136	357.990	0.004	361.208	0.006	360.429	0.007	359.221	0.005
40	1.0	51.265	53.215	0.013	54.812	0.023	53.619	0.029	52.113	0.022
40	1.5	72.537	71.235	0.009	72.242	0.019	70.953	0.019	69.361	0.016
40	2.0	110.707	106.862	0.006	108.041	0.011	106.654	0.029	105.105	0.039
40	2.5	178.269	173.589	0.003	174.002	0.009	172.470	0.008	170.818	0.006

TABLE III. *First–seventh columns:* Results for the short range Widom representation of the logarithm of cavity distribution function, i.e., $\ln[y(x)] = y_0 + y_2x^2 + y_4x^4 + \mathcal{O}[x^6]$, for all the 16 YOCP state points of interest. The low mean absolute relative deviations $e_{\ln y} < 0.53\%$ between the MD extracted $\ln[y(x)]$ and the truncated Widom series reveal that the first three terms suffice. Note the monotonic dependence of the y_0, y_2, y_4 coefficients on the normalized coupling parameter Γ/Γ_m and screening parameter κ . *Eighth–ninth columns:* Results of the ultra-long cavity simulation matching procedure for all the 16 YOCP state points. Matching in the overlapping interval $I_5 \cap I = [1.25, 1.4]$, where $I = I_4 \cup I_3 \cup I_2 \cup I_1 = [0.0, 1.4]$, leads to the constant $\ln C$. The extremely low mean absolute relative deviations $e_{\ln C} (< 0.005\%)$ again confirm the theoretical expectation that the ratio $\ln[y(r)/y_{\text{sim}}(r)]$ is well-approximated by a constant.

$\Gamma_{\text{ISO}}^{\text{OCP}}$	κ	Γ	y_0	y_2	y_4	$e_{\ln y} (\%)$	$\ln C$	$e_{\ln C} (\%)$
160	1.0	205.061	76.78	−29.49	4.06	0.12	199.864	0.002
160	1.5	286.437	59.00	−25.76	3.89	0.20	281.238	0.001
160	2.0	435.572	47.68	−22.84	3.71	0.29	430.361	0.001
160	2.5	708.517	40.18	−20.79	3.64	0.44	703.303	0.001
120	1.0	153.796	57.95	−22.20	3.05	0.12	148.600	0.002
120	1.5	215.930	44.88	−19.46	2.89	0.18	210.729	0.001
120	2.0	328.816	36.54	−17.44	2.83	0.30	323.611	0.001
120	2.5	534.722	31.01	−16.01	2.81	0.45	529.507	0.001
80	1.0	102.531	38.97	−14.83	2.01	0.12	97.349	0.003
80	1.5	144.330	30.51	−13.24	1.99	0.21	139.137	0.002
80	2.0	219.972	25.07	−11.94	1.94	0.32	214.771	0.001
80	2.5	357.136	21.46	−11.02	1.92	0.43	351.926	0.003
40	1.0	51.265	19.84	−7.51	1.01	0.13	46.100	0.005
40	1.5	72.537	15.82	−6.82	1.01	0.20	67.364	0.003
40	2.0	110.707	13.37	−6.52	1.11	0.53	105.519	0.002
40	2.5	178.269	11.52	−5.88	1.01	0.42	173.073	0.001

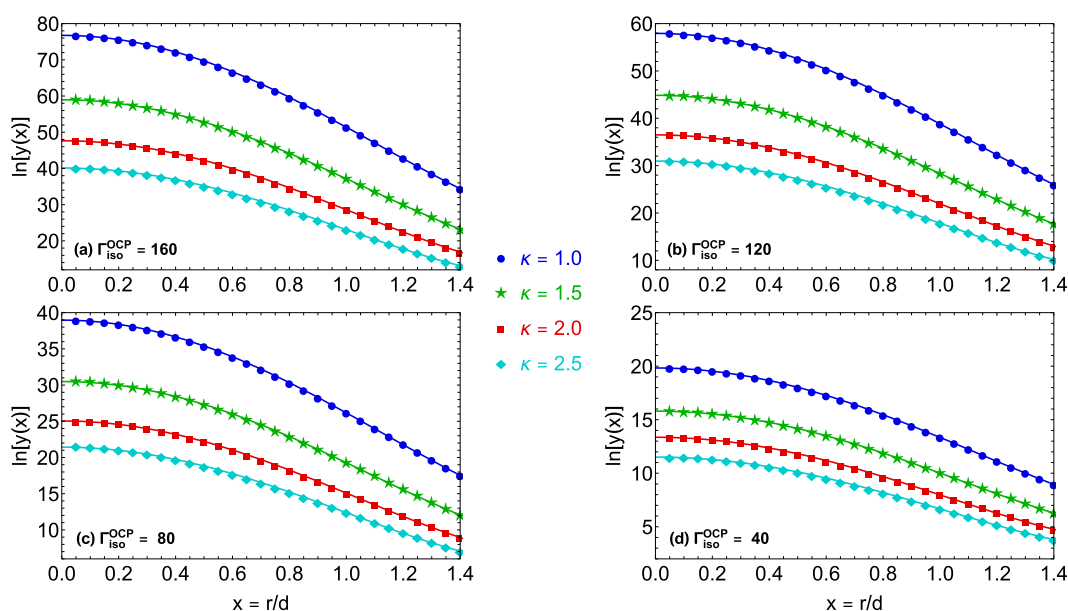


FIG. 5. Logarithm of the YOCP cavity distribution function within the correlation void as computed with static correlation input from the *long cavity MD simulations*. Results along the (a) $\Gamma_{\text{ISO}}^{\text{OCP}} = 160$ isomorph ($\kappa = 1.0, 1.5, 2.0, 2.5$), (b) $\Gamma_{\text{ISO}}^{\text{OCP}} = 120$ isomorph ($\kappa = 1.0, 1.5, 2.0, 2.5$), (c) $\Gamma_{\text{ISO}}^{\text{OCP}} = 80$ isomorph ($\kappa = 1.0, 1.5, 2.0, 2.5$), and (d) $\Gamma_{\text{ISO}}^{\text{OCP}} = 40$ isomorph ($\kappa = 1.0, 1.5, 2.0, 2.5$). The $\ln[y(r/d)]$ curves as obtained from the MD simulations (discrete symbols) and the Widom expansion with the least square fitted coefficients reported in Table III (solid lines). It is evident that the first three terms of the Widom expansion provide a very accurate representation of $\ln[y(r/d)]$ within the correlation void. The MD results, which are extracted every $0.002d$ with the histogram method, have been down-sampled for the purposes of illustration.

found to be $A_1(\Gamma, \kappa) = (25-360)$ depending on the state point, $A_2 = 20$, $A_3 = -0.1$, and $A_4 = 1.5$. The matching procedure, which was followed in the overlapping extent of $I_5 \cap I$, led to very accurate proportionality constants C that are documented in the last two columns of Table III. Figure 6 reveals how the Widom series representation of the biasing potential leads to nearly uniform tagged pair statistics and confirms that the chosen statistical sample size suffices for the accurate computation of the bridge function in nearly the full extent of the correlation void.

Our version of the cavity simulation method was successfully benchmarked against published results for dense simple liquids. In particular, the short range bridge functions were compared with tabulated MC and MD simulation data for Lennard-Jones fluids^{12,13} and tabulated MC simulation data for inverse power law systems.¹⁶ Our MD results always nearly overlapped with the literature results with the exception of minor deviations that lied well within the estimated uncertainties. Such validation exercise was not possible for Yukawa systems, since only MC generated short range screening potentials and not bridge functions are available.³¹

C. The numerical results

The short range bridge functions $B(r/d)$ and potentials of mean force $-\ln[g(r/d)]$ as computed from the application of the cavity distribution method with input from the ultra-long cavity MD simulations are shown in Fig. 7 for the 4 isomorph lines and 16 YOCP

state points of interest. The bridge functions, together with error bars, are also shown in Fig. 8 along different sub-intervals of the correlation void. Note that the comprehensive analysis of uncertainty propagation in the cavity distribution method, which led to the determination of the bridge function error bar levels, is detailed in Sec. III of the [supplementary material](#).

It is evident that the reduced-unit bridge function is strongly invariant within the correlation void along any YOCP isomorph curve. The observed degree of bridge function isomorph invariance is high enough that zoom-ins on different sub-intervals are necessary to discern the small $B(r/d)$ deviations between the different members of the same isomorph. Regardless of the YOCP isomorph, it is apparent from Fig. 8 that the $\kappa = 1.5, 2.0, 2.5$ members have nearly overlapping bridge functions, while the $\kappa = 1.0$ member has a slightly displaced bridge function. By inspecting the bridge functions of the $\kappa = 1.5, 2.0, 2.5$ members for each isomorph, it is deduced that error levels are comparable to the isomorph deviations observed. However, by inspecting the bridge function of the $\kappa = 1.0$ member with respect to those of the $\kappa = 1.5, 2.0, 2.5$ members, it is evident that the uncertainties are too minuscule to account even for the small deviations observed. Overall, it is concluded that similar to the intermediate and the long range, the observed isomorph invariance of the Yukawa bridge functions in the short range is only of approximate nature. In terms of absolute numbers, the degree of isomorph invariance is roughly similar outside and inside the correlation void. In terms of relative numbers, the degree of

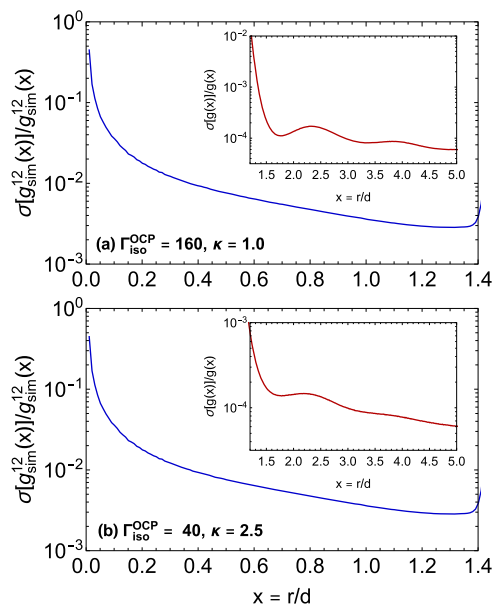


FIG. 6. Results for the YOCP state points (a) $\Gamma_{\text{ISO}}^{\text{OCP}} = 160$, $\kappa = 1.0$ and (b) $\Gamma_{\text{ISO}}^{\text{OCP}} = 40$, $\kappa = 2.5$. Main figure: Relative standard errors $\sigma[g_{\text{sim}}^{12}(r)]/g_{\text{sim}}^{12}(r)$ in the extraction of the radial distribution function of the tagged particle pair $g_{\text{sim}}^{12}(r)$ from ultra-long cavity MD simulations ($N = 1000$, $M_3 = 2^{25}$) within the short range $r \leq 1.4d$. Inset plot: Relative standard errors $\sigma[g(r)]/g(r)$ in the extraction of the radial distribution function $g(r)$ of the targeted system from standard NVT MD simulations ($N = 54872$, $M = 2^{16}$) in the intermediate range $1.25 \leq r/d \leq 5.00$. The error level $\sigma[g_{\text{sim}}^{12}(r)]/g_{\text{sim}}^{12}(r) \sim 0.01$ that emerges from the ultra-long cavity simulations is small enough to guarantee a reliable computation of the bridge function in the short range and is comparable to the error level of $\sigma[g(r)]/g(r)$ in the overlapping interval of $1.25 \leq r/d < 1.4$. As the distance decreases, the error level slowly increases up to $r \sim 0.2d$, then it begins to steeply increase, and finally becomes too high for $r < 0.05d$. This suggests that large bridge function uncertainties are localized close to the origin $r = 0$. The achieved tagged pair statistics are nearly uniform in the interval $0.2 \leq r/d \leq 1.4$.

isomorph invariance is much higher in the short range, as a result of the much higher bridge function magnitude within the correlation void.

The bridge function invariance suggests that the isomorph variant short range features of the positive cavity distribution function $\ln[y(r/d)]$ (see Fig. 5) and of the negative direct correlation function $c(r/d)$ (see Fig. 3) cancel each other out to a large extent, when these static correlations are added for the computation of the bridge function, see Eq. (6). It is important to note that the invariance level is nearly independent of the distance within the entire correlation void, since the relative $B(r)$ deviations between isomorph state points vary within 2%–7% for $0 < r/d \leq 1.4$ (using the $\kappa = 1.0$ member as the reference state). It is also worth pointing out that, for a given reduced distance, our methodology leads to uncertainties in the bridge function that are nearly independent of the state point, which implies that the relative errors in the bridge function are largest along the $\Gamma_{\text{ISO}}^{\text{OCP}} = 40$ isomorph where the bridge function magnitude is smallest. This expectation is confirmed

in Figs. 8(a), 8(d), 8(g), and 8(j). Furthermore, the large bridge function uncertainties that should arise near the origin, as anticipated from the enhanced $\sigma[g_{\text{sim}}^{12}(r)]/g_{\text{sim}}^{12}(r)$ error level recorded close to $r = 0$ (see Fig. 6), manifest themselves in the loss of $B(r)$ smoothness and the emergence of spiky saw-toothed $B(r)$ features at $r \lesssim 0.05d$.

On the other hand, the reduced-unit potential of mean force is strongly variant within the correlation void along any YOCP isomorph curve. Notice that the inset plots of Fig. 7 use logarithmic vertical scales in order to accommodate the five orders of magnitude change in the $\ln[g(r)]$ values that takes place from the edge of the correlation void up to the neighborhood of the origin, where it ultimately diverges. The $\ln[g(r/d)]$ deviations between different members of the same isomorph even exceed one order of magnitude and monotonically increase toward the origin. The above demonstrates that the $g(r/d)$ deviations between different members of the same isomorph are dramatic within the correlation void, in stark contrast to the isomorph invariance of $g(r/d)$ outside the correlation void. This was expected from the $g(r/d)$ deviations observed between isomorph state points at the edge of the correlation void, $1.25 \leq r/d \leq 1.4$, which is reliably probed by the OZ inversion method, see Sec. V.

Finally, for any YOCP state point and within the entire correlation void, the bridge function can be well approximated with a fourth degree polynomial, i.e., $B(x) = \sum_{i=0}^4 b_i x^i$. The mean absolute relative errors of such fits are $\sim 0.5\%$ regardless of the state point. This observation is important in view of attempts to parameterize the dependence of the YOCP bridge function on the (Γ, κ) state point or attempts to characterize the approximately isomorph YOCP bridge function exclusively through the reduced excess entropy s_{ex} . This task is beyond the scope of the present work, but it will be actively pursued in the future. It is worth noting that such polynomial fits were first employed for the bridge function of hard-sphere systems.⁸² Note that, in contrast to the logarithm of the cavity distribution function, the short range bridge function cannot be accurately fitted with the Widom even polynomial expansion, which leads to mean absolute relative errors that exceed $\sim 7\%$. In view of Eq. (6), this should be attributed to the small-argument expansion of the direct correlation function $c(r)$. In fact, the analytical solution of the soft mean spherical approximation for the direct correlation function within the correlation void contains odd polynomial terms for the YOCP ($\propto x, x^3$) and odd and even terms for the OCP ($\propto x^2, x^3, x^5$).^{80,81}

D. The extrapolation at the origin

In the histogram method, the effective bin position lies at the center of each bin. As a result, the cavity distribution method can be utilized for the computation of the short range bridge function values only at distances larger than $\Delta r/2$ ($= 0.001d$ in our case), which implies that the value of the bridge function at the origin remains inaccessible. A rigorous small-argument expansion is not available for the bridge function, which suggests that an extrapolation based on the functional behavior of the bridge function at very short distances might lead to erroneous values, especially given the large bridge function uncertainties in the vicinity of $r = 0$. Nevertheless, the Widom even polynomial expansion for the cavity distribution function⁷⁹ can be utilized for extrapolation purposes. According

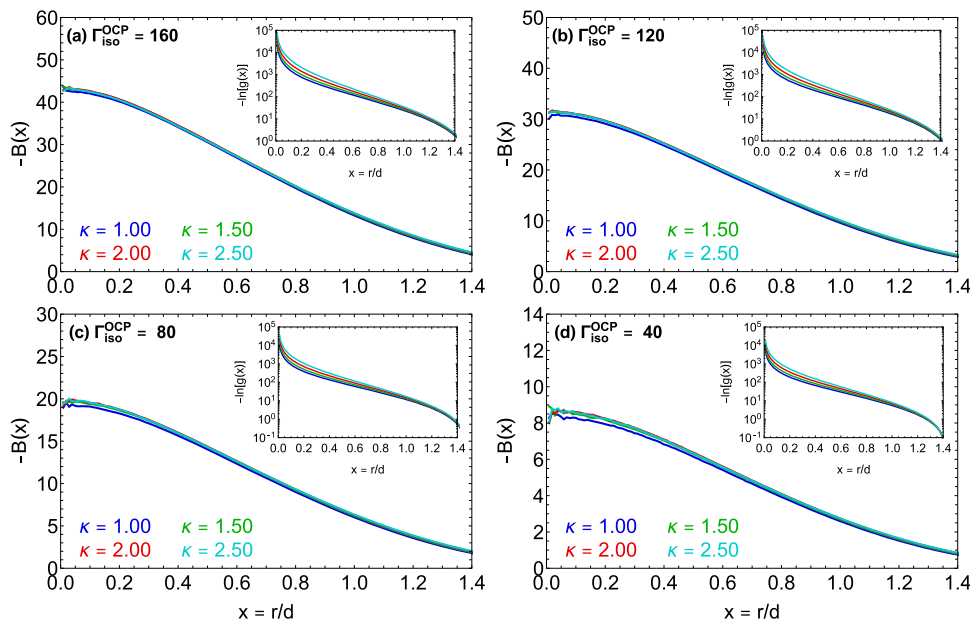


FIG. 7. YOCP bridge functions (main) and potentials of mean force (inset) within the correlation void $r/d \leq 1.4$ as computed with the cavity distribution method with input from *ultra-long cavity MD simulations*. Results for the (a) four members of the $\Gamma_{\text{iso}}^{\text{OCP}} = 160$ isomorph ($\kappa = 1.0, 1.5, 2.0, 2.5$), (b) four members of the $\Gamma_{\text{iso}}^{\text{OCP}} = 120$ isomorph ($\kappa = 1.0, 1.5, 2.0, 2.5$), (c) four members of the $\Gamma_{\text{iso}}^{\text{OCP}} = 80$ isomorph ($\kappa = 1.0, 1.5, 2.0, 2.5$), and (d) four members of the $\Gamma_{\text{iso}}^{\text{OCP}} = 40$ isomorph ($\kappa = 1.0, 1.5, 2.0, 2.5$).

to Eq. (6), this would require knowledge of the direct correlation function at the origin. Despite the absence of a small-argument expansion for the direct correlation function, its magnitude at the origin $r = 0$ can be computed by taking advantage of the two exact relations of the integral equation theory together with $g(0) = 0$ that is valid for origin divergent pair interactions as those realized in YOCP systems.

The theoretical foundation of the present bridge function extrapolation method strongly resembles that of the so-called zero separation theorems.^{51,83} We set $r = 0$ in the Ornstein–Zernike equation, see Eq. (3), and employ $h(0) = -1$. Solving for $c(r = 0)$, we acquire

$$c(0) = -1 - n \int c(r)h(r)d^3r,$$

where we set $\mathbf{r}' = \mathbf{r}$ for the dummy volume integration variable. After substituting for $h(r) = g(r) - 1$ and splitting the integral, the statistical relation for the reduced inverse isothermal compressibility $\mu_T = 1 - n/c(r)d^3r$ emerges. By adding and then subtracting the asymptotic limit of the direct correlation function $-\beta u(r)$ in the respective factor of the integrand, the reduced excess internal energy $u_{\text{ex}} = (1/2)n\beta \int g(r)u(r)d^3r$ emerges. The remaining integral can be simplified by utilizing spherical coordinates and normalized distance units $x = r/d$. The above leads to

$$c(0) = -\mu_T + 2u_{\text{ex}} - 3 \int_0^\infty x^2 g(x)[c(x) + \beta u(x)]dx.$$

We proceed with setting $r = 0$ in the non-linear closure equation, Eq. (4), and we employ $h(0) = -1$. The singularities of the

interaction potential and of the potential of mean force at the origin can be removed by combining the two diverging terms for the finite valued logarithm of the cavity distribution function $\ln[y(0)]$ to emerge, whose value at the origin is given by the zero-order term of the Widom expansion y_0 . Thus, we have

$$B(0) = y_0 + c(0) + 1.$$

Finally, we combine the above equations and we also set $\delta = 3 \int_0^\infty x^2 g(x)[c(x) + \beta u(x)]dx$ to end up with

$$B(0) = y_0 - \mu_T + 2u_{\text{ex}} - \delta + 1. \quad (12)$$

All four contributions to $B(0)$ can be easily determined from available MD simulations: u_{ex} from the canonical mean of total potential energies, μ_T from the hypervirial route,⁸⁴ δ by combining the Ornstein–Zernike equation with simulation extracted radial distribution functions, and y_0 by least square fitting the output of cavity simulations within the correlation void to the first three terms of the Widom series. Note that tail corrections in the evaluation of u_{ex} , μ_T due to the truncation of the Yukawa potential are negligible. Note also that the more accurate y_0 values resulting from the ultra-long cavity simulations should be preferred over the y_0 values that resulted from the long cavity simulations and are reported in Table III.

The $B(0)$ values that result from the above extrapolation method are collected in Table IV. None of the contributing

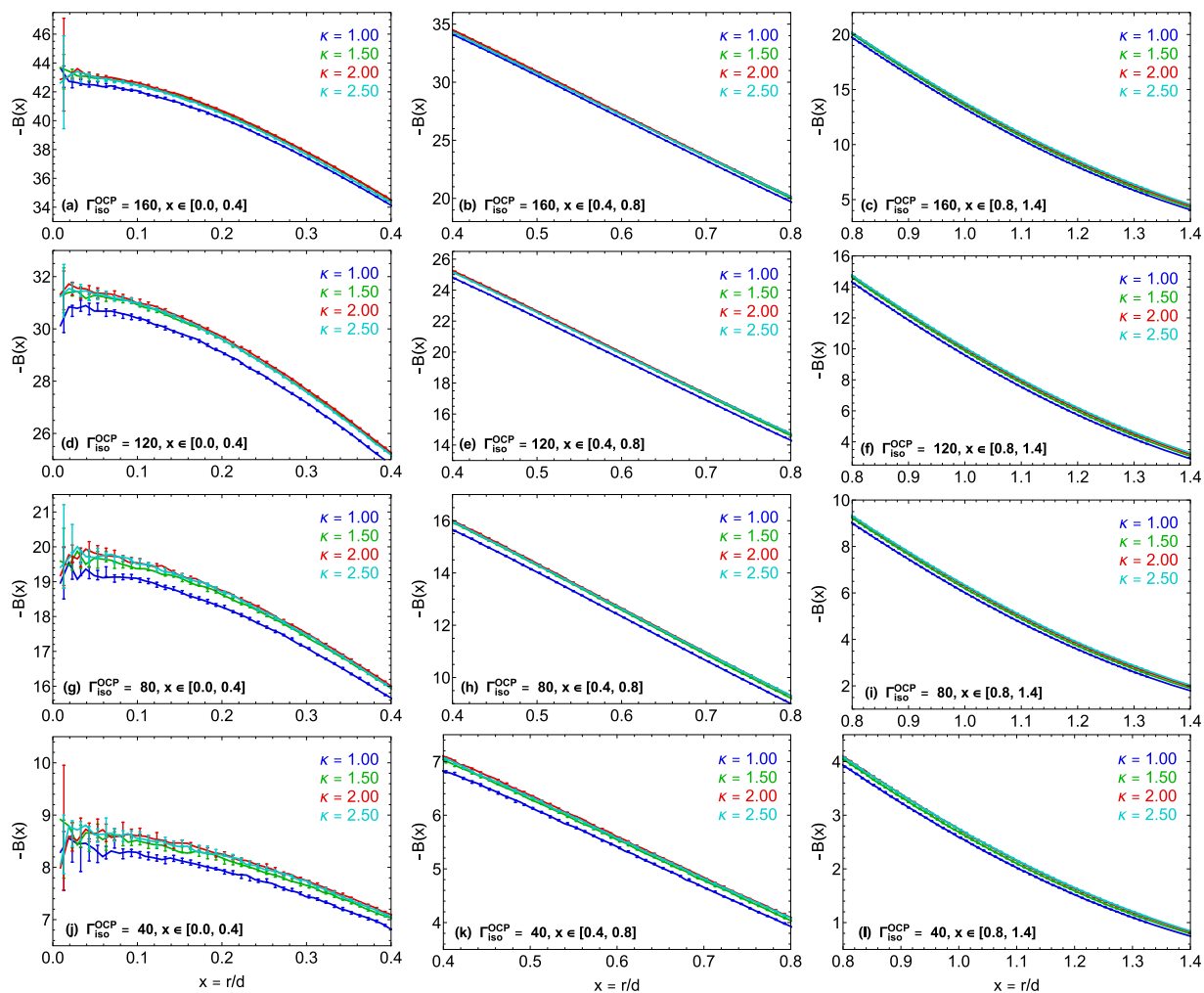


FIG. 8. YOCP bridge functions, including error bars, within different sub-intervals of the correlation void $r/d \leq 1.4$ as computed with the cavity distribution method with input from *ultra-long cavity MD simulations*. Results for the (a)–(c) four members of the $\Gamma_{\text{iso}}^{\text{OCP}} = 160$ isomorph ($\kappa = 1.0, 1.5, 2.0, 2.5$) in sub-intervals $[0, 0.4d]$, $[0.4d, 0.8d]$, and $[0.8d, 1.4d]$, (d)–(f) four members of the $\Gamma_{\text{iso}}^{\text{OCP}} = 120$ isomorph ($\kappa = 1.0, 1.5, 2.0, 2.5$) in sub-intervals $[0, 0.4d]$, $[0.4d, 0.8d]$, and $[0.8d, 1.4d]$, (g)–(i) four members of the $\Gamma_{\text{iso}}^{\text{OCP}} = 80$ isomorph ($\kappa = 1.0, 1.5, 2.0, 2.5$) in sub-intervals $[0, 0.4d]$, $[0.4d, 0.8d]$, and $[0.8d, 1.4d]$, and (j)–(l) four members of the $\Gamma_{\text{iso}}^{\text{OCP}} = 40$ isomorph ($\kappa = 1.0, 1.5, 2.0, 2.5$) in sub-intervals $[0, 0.4d]$, $[0.4d, 0.8d]$, and $[0.8d, 1.4d]$. The isomorph deviations and especially the error bars are very small and can be better discerned in the zero-separation vicinity.

quantities $(y_0, \mu_T, u_{\text{ex}}, \delta)$ are isomorph invariant: y_0 due to its deep connection with the excess chemical potential,^{51,83} μ_T because its thermodynamic definition involves volume derivatives,⁴⁷ u_{ex} owing to its straightforward connection with the interaction potential (see also the Rosenfeld–Tarazona decomposition⁴⁵), and δ due to the presence of the direct correlation function in the integrand. The isomorph variance is confirmed in Table IV, where large differences can be observed in the above quantities among isentropic YOCP state points. Despite that the $(y_0, \mu_T, u_{\text{ex}}, \delta)$ contributing quantities are not isomorph invariant, the bridge function at the origin is revealed to be isomorph invariant to a high degree, as expected

from the $B(r)$ invariance in the statistically sampled range. In fact, a simple quadratic extrapolation of the bridge function in the smooth interval $0.05 < r/d < 0.4$ would result in very similar but slightly less accurate values of $B(0)$. Finally, we note that specially designed simulations based on the insertion of test particles can be utilized in order to extract $\ln[y(0)] = y_0$ exactly at the origin, thus avoiding the need for any extrapolation.⁸⁵ However, due to the very high number of statistically independent configurations sampled in the ultra-long cavity simulations, the extrapolated $B(0)$ values are accurate enough so that an additional series of simulations are judged to be redundant.

TABLE IV. Extrapolated value of the bridge function at the origin, $B(0)$, together with all four distinct contributions to its magnitude according to Eq. (12), for the 16 YOCP state points of interest. The reduced excess internal energy u_{ex} , the reduced inverse isothermal compressibility μ_T , and the integral residual term δ are either extracted directly or computed with input from ultra-accurate standard MD simulations ($N = 54\,872$, $M = 2^{16}$). The zero-order term of the Widom expansion y_0 is computed by least square fitting input from ultra-long cavity simulations ($N = 1000$, $M_3 = 2^{25}$) within the short range $r/d \leq 1.4$. There are minor deviations $\ll 1\%$ between the y_0 values that are extrapolated from the ultra-long cavity simulations and those that are extrapolated from the long cavity simulations (see Table III) owing to the different statistically independent configurations sampled ($M_3 = 2^{25}$ vs $M_2 = 2^{20}$). The contribution of the integral residual term δ to $B(0)$ is the smallest for all 16 state points, as expected by the fact that the direct correlation function approaches its asymptotic limit already around $r \simeq 2d$ and the fact that the correlation void $g(r) \simeq 0$ begins around $r \simeq 1.4d$, which imply that the integrand factor $g(x)[c(x) + \beta u(x)]$ is non-zero only within a fraction of the first coordination cell $1.4 \leq r/d \leq 2$.

Γ_{ISO}^{OCP}	κ	Γ	$B(0)$	y_0	μ_T	u_{ex}	δ
160	1.0	205.061	-42.791	76.766	540.296	206.148	-7.444
160	1.5	286.437	-43.324	58.963	284.173	88.661	-3.565
160	2.0	435.572	-43.485	47.667	193.548	48.474	-4.449
160	2.5	708.517	-43.393	40.140	150.459	30.558	-4.812
120	1.0	153.796	-30.940	57.922	405.692	155.043	-5.745
120	1.5	215.930	-31.511	44.885	215.176	67.267	-3.246
120	2.0	328.816	-31.670	36.545	146.766	37.025	-3.501
120	2.5	534.722	-31.658	30.966	114.437	23.494	-3.824
80	1.0	102.531	-19.382	38.977	271.054	103.863	-3.969
80	1.5	144.330	-19.785	30.483	144.489	45.467	-2.287
80	2.0	219.972	-19.948	25.046	99.007	25.276	-2.462
80	2.5	357.136	-19.955	21.442	77.391	16.199	-2.598
40	1.0	51.265	-8.3897	19.842	136.347	52.530	-2.055
40	1.5	72.537	-8.6413	15.798	73.552	23.451	-1.211
40	2.0	110.707	-8.7334	13.279	50.936	13.320	-1.283
40	2.5	178.269	-8.7523	11.534	40.021	8.684	-1.366

VII. SUMMARY AND DISCUSSION

Bridge functions of dense Yukawa liquids were systematically computed aiming to confirm or disprove the validity of the conjecture of reduced unit bridge function invariance along isomorphs, i.e., phase diagram lines of constant excess entropy. 16 state points were selected that belong to four isomorphs and cover the entire dense liquid YOCP phase diagram up to the vicinity of the liquid–solid (bcc/fcc) phase transition. The YOCP isomorph curves were traced out with the small step method as well as with the direct isomorph check. Intermediate and long range bridge functions were made accessible after application of the Ornstein–Zernike inversion method with radial distribution function input from ultra-accurate standard canonical molecular dynamics simulations that employed carefully selected parameters, while short range bridge functions were made accessible after application of the cavity distribution method with structural input from ultra-long specially designed canonical molecular dynamics simulations featuring a tagged particle pair. Results confirmed that the YOCP bridge functions are isomorph invariant to a very high degree, but their invariance was concluded to be approximate, since the small deviations observed between isentropic bridge functions always exceeded the quantified uncertainty levels. The short range bridge function invariance constitutes a surprising outcome, given that all other static two-particle correlation functions are strongly variant within the correlation void.

A detailed methodology was developed for the design of the tagged pair interaction potential that leads to the acquisition of approximately uniform pair statistics in the whole correlation void based on an algorithmic approach. The externally controlled tagged pair potential was decomposed into windowing and biasing components. The windowing component constrained the tagged pair within overlapping sub-intervals of the correlation void without affecting their correlations within each confinement range and was realized with the aid of two error functions. The biasing component ensured statistical uniformity within each window and was determined by successive approximations with input from cavity simulations of increasing duration, starting from a Gaussian series representation of increasing complexity and culminating into a Widom even series representation. Since poor statistics at an extremely short distance are rather unavoidable with the cavity distribution method, an extrapolation technique was developed in order to determine the value of the bridge function at the origin. It was based on well-known algebraic manipulations of the Ornstein–Zernike integral equation and of the non-linear closure condition that were originally employed in the derivation of the so-called zero-separation theorems. It capitalized on the high accuracy of the Widom expansion for the cavity logarithm in order to provide a reliable extrapolation.

The computed YOCP bridge functions within the non-asymptotic range are illustrated in Fig. 9 for the 4 isomorph curves and 16 state points of interest. The very high degree of the still

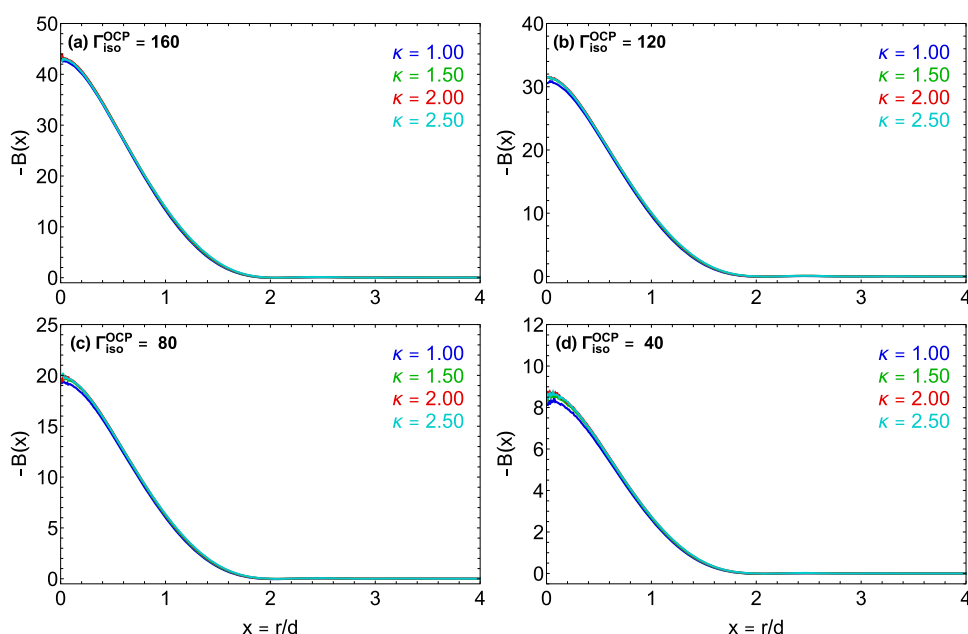


FIG. 9. “Exact” bridge functions of dense YOCP liquids in the entire non-trivial range of reduced distances. (a)–(d) Results for the four members ($\kappa = 1.0, 1.5, 2.0, 2.5$) of the $\Gamma_{\text{iso}}^{\text{OCP}} = 160, 120, 80, 40$ isomorphs, respectively. Short range bridge functions $r/d \leq 1.4$ are computed by applying the cavity distribution method with input from *ultra-long canonical MD cavity simulations*, while intermediate and long range bridge functions $r/d \geq 1.25$ are computed by applying the Ornstein–Zernike inversion method with input from *ultra-accurate canonical MD simulations*. The overlapping interval $1.25 \leq r/d \leq 1.4$ is utilized to re-normalize the short range bridge functions, which are computed within an arbitrary additive constant by the cavity distribution method.

approximate bridge function isomorph invariance is apparent in the entire range. Tabulated full range Yukawa bridge functions for these 16 state points, organized per isomorph curve, are available in the [supplementary material](#). Specifically, raw bridge function data are provided in the interval $0.01d < r \leq 5d$ in steps of $0.01d$, i.e., the data have been down-sampled by five given the $\Delta r = 0.002d$ bin width employed in the histogram methods for the extraction of the cavity distribution function (inside the correlation void) and the radial distribution function (outside the correlation void). Note that the starting $r = 0.01d$ distance is missing from the dataset for all state points, since it was judged to be poorly sampled even by the ultra-long cavity simulations.

The investigation has demonstrated that YOCP bridge functions are isomorph invariant to a very high—yet still approximate—degree in the entire non-trivial range. Therefore, the sole conjecture of the isomorph-based empirically modified hypernetted-chain (IEMHNC) approximation has been verified for Yukawa systems rationalizing the remarkable agreement of the IEMHNC structural and thermodynamics properties with the “exact” results of computer simulations. It is expected with confidence that the approximate isomorph invariance of bridge functions holds for any R-simple system. However, the degree of isomorph invariance should vary between systems depending on the strength of the virial potential–energy correlations, which is exceptionally high for Yukawa systems. Hence, similar studies should be carried out for other R-simple liquids, e.g., for Lennard-Jones⁸⁶ or pure exponential repulsive systems.^{62,87} In addition, some types of isomorph invariance concerning quantities that are linked to quasi-universal behavior such as the excess entropy scaling of transport coefficients^{47,48} have been observed to apply also to few systems that do not have strong enough virial potential–energy correlations^{88–90} to be classified as R-simple. Thus, it is also important to check whether an

approximate isentropic invariance of bridge functions holds for systems that are not R-simple.

Despite that the bridge function constitutes one of the most important and certainly the most enigmatic static two-particle correlation functions, few of its exact or even approximate properties have been so far discovered. The approximate isomorph invariance for R-simple systems can now be added to this short list. Apart from its general theoretical value and the fact that it is the building block of the successful IEMHNC approach, the isomorph invariance property has additional practical value: In general, closed-form parameterizations of the bridge function have proven to be rather elusive due to the difficulty of fitting a function of three independent variables that is anyway formidable to calculate based on first principles. To our knowledge, analytical bridge functions are currently available only for few inverse power law systems,^{16,19,82} since these systems require a single independent variable for the complete specification of each thermodynamic state. The approximate property of isomorph invariance suggests that the bridge functions of R-simple systems only depend on the reduced excess entropy and the reduced distance, paving the way for future parameterization studies.

SUPPLEMENTARY MATERIAL

See the [supplementary material](#) for a meticulous analysis of uncertainty propagation during indirect bridge function extraction with the Ornstein–Zernike inversion method and the cavity distribution method. Moreover, tabulations of the raw data for the Yukawa bridge functions of the 16 state points of interest (equally distributed among four isomorph curves) in the entire non-asymptotic range are also made available.

ACKNOWLEDGMENTS

The authors would like to acknowledge the financial support of the Swedish National Space Agency under Grant No. 143/16. This work was also partially supported by VILLUM Foundation under Grant No. 16515 (Matter). GPU molecular dynamics simulations were carried out at the *Glass and Time* computer cluster (Roskilde University). CPU molecular dynamics simulations were carried out on resources provided by the Swedish National Infrastructure for Computing (SNIC) at the NSC (Linköping University) partially funded by the Swedish Research Council through Grant Agreement No. 2016-07213.

DATA AVAILABILITY

The data that support the findings of this study are available within this article and its [supplementary material](#) and corresponding author upon reasonable request.

REFERENCES

- J. P. Hansen and I. R. McDonald, *Theory of Simple Liquids* (Academic Press, London, 2006).
- H. L. Frisch and J. L. Lebowitz, *The Equilibrium Theory of Classical Fluids* (Benjamin, New York, 1964).
- D. Chandler, *Introduction to Modern Statistical Mechanics* (Oxford University Press, New York, 1987).
- A. Santos, *A Concise Course on the Theory of Classical Liquids* (Springer, Heidelberg, 2016).
- P. Attard and G. N. Patey, *J. Chem. Phys.* **92**, 4970 (1990).
- C. Caccamo, *Phys. Rep.* **274**, 1 (1996).
- J. M. Bomont, *Adv. Chem. Phys.* **139**, 1 (2008).
- G. Torrie and G. N. Patey, *Mol. Phys.* **34**, 1623 (1977).
- S. Labík and W. R. Smith, *J. Chem. Phys.* **88**, 1223 (1988).
- J. Kolafa, S. Labík, and A. Malijevský, *Mol. Phys.* **100**, 2629 (2002).
- R. Fantoni and G. Pastore, *J. Chem. Phys.* **120**, 10681 (2004).
- M. Llano-Restrepo and W. G. Chapman, *J. Chem. Phys.* **97**, 2046 (1992).
- D. Tomazic, F. Hoffgaard, and S. M. Kast, *Chem. Phys. Lett.* **591**, 237 (2014).
- D. M. Duh and A. D. J. Haymet, *J. Chem. Phys.* **103**, 2625 (1995).
- I. Vyalov, G. Chuev, and N. Georgi, *J. Chem. Phys.* **141**, 074505 (2014).
- M. Llano-Restrepo and W. G. Chapman, *J. Chem. Phys.* **100**, 5139 (1994).
- M. Llano-Restrepo and W. G. Chapman, *Int. J. Thermophys.* **16**, 319 (1995).
- P. D. Poll, N. W. Ashcroft, and H. E. DeWitt, *Phys. Rev. A* **37**, 1672 (1988).
- H. Iyetomi, S. Ogata, and S. Ichimaru, *Phys. Rev. A* **46**, 1051 (1992).
- S. Ogata, *Phys. Rev. E* **53**, 1094 (1996).
- D. L. Cheung, L. Anton, M. P. Allen, and A. J. Masters, *Phys. Rev. E* **73**, 061204 (2006).
- E. Lomba, M. Alvarez, G. Stell and J. A. Anta, *J. Chem. Phys.* **97**, 4349 (1992); S. Kambayashi and J. Chihara, *Phys. Rev. E* **50**, 1317 (1994).
- D. M. Duh and A. D. J. Haymet, *J. Chem. Phys.* **97**, 7716 (1992).
- C. Tasseven, L. E. Gonzalez, M. Silbert, O. Alcaraz, and J. Trullas, *J. Chem. Phys.* **115**, 4676 (2001).
- J. Puibasset and L. Belloni, *J. Chem. Phys.* **136**, 154503 (2012).
- L. Belloni, *J. Chem. Phys.* **147**, 164121 (2017).
- P. Tolia and F. Lucco Castello, *Phys. Plasmas* **26**, 043703 (2019).
- F. Lucco Castello, P. Tolia, J. S. Hansen, and J. C. Dyre, *Phys. Plasmas* **26**, 053705 (2019).
- F. Lucco Castello and P. Tolia, "On the advanced integral equation theory description of dense Yukawa one-component plasma liquids," *Contrib. Plasma Phys.* (published online, 2020).
- To our knowledge, the bridge functions of Yukawa systems have not been computed before from simulations. Screening potentials have been computed from MC simulations,³¹ but they differ from bridge functions since they do not involve the direct correlation functions.
- J. M. Caillol and D. Gilles, *J. Phys. A: Math. Gen.* **36**, 6243 (2003).
- V. E. Fortov, A. V. Ivlev, S. A. Khrapak, A. G. Khrapak, and G. E. Morfill, *Phys. Rep.* **421**, 1 (2005).
- Z. Donkó, G. J. Kalman, and P. Hartmann, *J. Phys.: Condens. Matter* **20**, 413101 (2008).
- G. E. Morfill and A. V. Ivlev, *Rev. Mod. Phys.* **81**, 1353 (2009).
- M. Bonitz, C. Henning, and D. Block, *Rep. Prog. Phys.* **73**, 066501 (2010).
- H. M. Thomas, M. Schwabe, M. Y. Pustyl'nik, C. A. Knapek *et al.*, *Plasma Phys. Controlled Fusion* **61**, 014004 (2019).
- H. Boroudjerdi, Y.-W. Kim, A. Naji, R. R. Netz *et al.*, *Phys. Rep.* **416**, 129 (2005).
- N. Gnan, T. B. Schröder, U. R. Pedersen, N. P. Bailey, and J. C. Dyre, *J. Chem. Phys.* **131**, 234504 (2009).
- T. S. Ingebrigtsen, T. B. Schröder, and J. C. Dyre, *Phys. Rev. X* **2**, 011011 (2012).
- J. C. Dyre, *Phys. Rev. E* **88**, 042139 (2013).
- J. C. Dyre, *J. Phys.: Condens. Matter* **28**, 323001 (2016).
- T. B. Schröder and J. C. Dyre, *J. Chem. Phys.* **141**, 204502 (2014).
- N. P. Bailey, U. R. Pedersen, N. Gnan, T. B. Schröder, and J. C. Dyre, *J. Chem. Phys.* **129**, 184507 (2008).
- A. A. Veldhorst, T. B. Schröder, and J. C. Dyre, *Phys. Plasmas* **22**, 073705 (2015).
- Y. Rosenfeld and P. Tarazona, *Mol. Phys.* **95**, 141 (1998); Y. Rosenfeld, *Phys. Rev. E* **62**, 7524 (2000).
- T. S. Ingebrigtsen, A. A. Veldhorst, T. B. Schröder, and J. C. Dyre, *J. Chem. Phys.* **139**, 171101 (2013).
- Y. Rosenfeld, *Phys. Rev. A* **15**, 2545 (1977); *J. Phys.: Condens. Matter* **13**, L39 (2001).
- J. C. Dyre, *J. Chem. Phys.* **149**, 210901 (2018).
- Y. Rosenfeld, *J. Stat. Phys.* **42**, 437 (1986).
- Y. Rosenfeld and N. W. Ashcroft, *Phys. Rev. A* **20**, 1208 (1979).
- Y. Rosenfeld, *Phys. Rev. A* **24**, 2805 (1981).
- Y. Rosenfeld, *J. Chem. Phys.* **103**, 9800 (1995).
- L. L. Lee, *J. Chem. Phys.* **97**, 8606 (1992).
- A. G. Vompe and G. A. Martynov, *J. Chem. Phys.* **100**, 5249 (1994).
- L. L. Lee, *J. Chem. Phys.* **103**, 9388 (1995).
- J. M. Bomont, N. Jakse, and J. L. Bretonnet, *J. Chem. Phys.* **107**, 8030 (1997).
- J. M. Bomont and J. L. Bretonnet, *J. Chem. Phys.* **114**, 4141 (2001).
- T. S. Ingebrigtsen, T. B. Schröder, and J. C. Dyre, *J. Phys. Chem. B* **116**, 1018 (2012).
- J. C. Dyre, *J. Phys. Chem. B* **118**, 10007 (2014).
- N. P. Bailey, L. Böhling, A. A. Veldhorst, T. B. Schröder, and J. C. Dyre, *J. Chem. Phys.* **139**, 184506 (2013).
- L. Costigliola, T. B. Schröder, and J. C. Dyre, *J. Chem. Phys.* **144**, 231101 (2016).
- A. K. Bacher, T. B. Schröder, and J. C. Dyre, *J. Chem. Phys.* **149**, 114502 (2018).
- L. Böhling, N. P. Bailey, T. B. Schröder, and J. C. Dyre, *J. Chem. Phys.* **140**, 124510 (2014).
- O. S. Vaulina and S. A. Khrapak, *J. Exp. Theor. Phys.* **90**, 287 (2000).
- O. Vaulina, S. Khrapak, and G. Morfill, *Phys. Rev. E* **66**, 016404 (2002).
- S. Hamaguchi, R. T. Farouki, and D. H. E. Dubin, *J. Chem. Phys.* **105**, 7641 (1996).
- S. Hamaguchi, R. T. Farouki, and D. H. E. Dubin, *Phys. Rev. E* **56**, 4671 (1997).
- U. R. Pedersen, L. Costigliola, N. P. Bailey, T. B. Schröder, and J. C. Dyre, *Nat. Commun.* **7**, 12386 (2016).
- S. A. Khrapak, B. A. Klumov, P. Huber, V. I. Molotkov *et al.*, *Phys. Rev. E* **85**, 066407 (2012).

- ⁷⁰R. E. Nettleton and M. S. Green, *J. Chem. Phys.* **29**, 1365 (1958).
- ⁷¹J. S. Perkyns, K. M. Dyer, and B. M. Pettitt, *J. Chem. Phys.* **116**, 9404 (2002).
- ⁷²S. Labík, H. Gabrielová, J. Kolafa, and A. Malijevský, *Mol. Phys.* **101**, 1139 (2003).
- ⁷³S. K. Kwak and D. A. Kofke, *J. Chem. Phys.* **122**, 104508 (2005).
- ⁷⁴L. Reatto, D. Levesque, and J. J. Weis, *Phys. Rev. A* **33**, 3451 (1986).
- ⁷⁵E. M. Apfelbaum, *Phys. Plasmas* **14**, 123703 (2007).
- ⁷⁶J. Vorberger and D. O. Gericke, *High Energy Density Phys.* **9**, 178 (2013).
- ⁷⁷N. P. Bailey, T. S. Ingebrigtsen, J. S. Hansen, A. A. Veldhorst *et al.*, *SciPost Phys.* **3**, 038 (2017).
- ⁷⁸S. Plimpton, *J. Comput. Phys.* **117**, 1 (1995).
- ⁷⁹B. Widom, *J. Chem. Phys.* **39**, 2808 (1963).
- ⁸⁰P. Tolias, S. Ratynskaia, and U. de Angelis, *Phys. Rev. E* **90**, 053101 (2014).
- ⁸¹P. Tolias, S. Ratynskaia, and U. de Angelis, *Phys. Plasmas* **22**, 083703 (2015).
- ⁸²A. Malijevsky and S. Labik, *Mol. Phys.* **60**, 663 (1987).
- ⁸³L. L. Lee and K. S. Shing, *J. Chem. Phys.* **91**, 477 (1989).
- ⁸⁴M. P. Allen and D. J. Tildesley, *Computer Simulation of Liquids* (Clarendon Press, Oxford, 1989).
- ⁸⁵J. R. Henderson, *Mol. Phys.* **48**, 389 (1983).
- ⁸⁶T. B. Schröder, N. Gnan, U. R. Pedersen, N. P. Bailey, and J. C. Dyre, *J. Chem. Phys.* **134**, 164505 (2011).
- ⁸⁷A. K. Bacher, T. B. Schröder, and J. C. Dyre, *J. Chem. Phys.* **149**, 114501 (2018).
- ⁸⁸J. R. Errington, T. M. Truskett, and J. Mittal, *J. Chem. Phys.* **125**, 244502 (2006).
- ⁸⁹W. P. Krekelberg, T. Kumar, J. Mittal, J. R. Errington, and T. M. Truskett, *Phys. Rev. E* **79**, 031203 (2009).
- ⁹⁰M. Agarwal, M. Singh, R. Sharma, M. Parvez Alam, and C. Chakravarty, *J. Phys. Chem. B* **114**, 6995 (2010).